Rational Design of the First Spherical Supramolecular Dendrimers Self-Organized in a Novel Thermotropic Cubic Liquid-Crystalline Phase and the Determination of Their Shape by X-ray Analysis

V. S. K. Balagurusamy,[†] G. Ungar,[†] V. Percec,*[,‡] and G. Johansson[‡]

Contribution from the Department of Engineering Materials and Centre for Molecular Materials, The University of Sheffield, Sheffield S1 3JD, UK, and The W. M. Keck Laboratories for Organic Synthesis, Department of Macromolecular Science, Case Western Reserve University, Cleveland, Ohio 44106-7202

Received September 19, 1996[⊗]

Abstract: The rational design, the synthesis *via* a new convergent approach, and the characterization of four generations of monodendrons based on the AB_3 building block methyl 3,4,5-trishydroxybenzoate are described. The first generation monodendrons are crystalline. The second generation methyl 3,4,5-tris-3′,4′,5′-[tris(*n*-dodecyloxy)benzyloxy]benzoate (**12Gn-AG-CH$_3$**, $n = 2$), the corresponding benzyl alcohol (**12G2-AG-CH$_2$OH**) and benzoic acid (**12G2-AG**), and all higher generation monodendrons with $n = 3$ and 4 exhibit in addition to the crystal phase an isomorphous cubic liquid-crystalline (LC) phase of $Pm\bar{3}n$ space group. The cubic unit cell parameters of **12G2-AG**, **12G3-AG**, and **12G4-AG** are 68.3, 79.2, and 84.0 Å, respectively. Computed electron density profiles demonstrated that in the cubic phase 12, 6, and 2 monodendrons of generation 2, 3 and 4 are self-assembled in supramolecular dendrimers resembling spherical micelles when they are centered at the corners and the body-center and respectively highly rounded tetrahedra when they are at $^1/_4$ and $^3/_4$ distance along one of the bisectors of each face of the cubic cell. This novel thermotropic LC phase is similar to that of the lyotropic $Pm\bar{3}n$ phase of biological lipids. These supramolecular dendrimers contain a poly(benzyl ether) core dispersed in an aliphatic matrix of nearly uniform density which is made up of the melted terminal long alkyl chains of the monodendrons. The size of the supramolecular dendrimer and of the entire unit cell increases with generation number as a result of a disproportionately large increase in the number of AB_3 repeat units relative to the number of terminal alkyl chains in a monodendron which decreases its average cone angle. The present experiments provide the first examples of monodendrons which self-assemble into spherical supramolecular dendrimers forming a thermotropic cubic LC phase.

Introduction

The discovery and subsequent expansion of research on dendrimers[1] produced a dramatic increase of our synthetic capabilities to design building blocks which enable for the first time the construction of complex macromolecular and supramolecular systems with controlled architectures, predictable and well defined shapes, functions, properties, and nanoscopic device fabrication potentiality.[2,3] The elaboration of the convergent method[4] for their preparation initiated efforts toward the development of accelerated synthetic techniques based on covalent[5] and supramolecular[6] chemistry approaches for the preparation of monodendrons and dendrimers. It is well accepted that dendrimers exhibit a spherical shape in solution.[1] However, less is known about their shape in melt and solid states although most of their new and unusual physical properties and functions in these states are determined by their shape. Various indirect techniques which cannot easily discriminate between single species and aggregates have strongly suggested that in solid and melt states dendrimers can adopt either spherical[1,6b,7] or rodlike shapes.[1,7c,8]

* Corresponding author: Phone: 216-368-4242. Fax: 216-368-4202. e-mail: vxp5@po.cwru.edu.

† The University of Sheffield.

‡ Case Western Reserve University.

⊗ Abstract published in *Advance ACS Abstracts,* February 1, 1997.

(1) For reviews on dendrimers, see: (a) Tomalia, D. A.; Durst, H. D. *Top. Curr. Chem.* **1993**, *165*, 193. (b) *Advances in Dendritic Macromolecules*; Newkome, G. R., Ed.; JAI Press, Inc.: Greenwich, 1994; Vol. 1, 1995; Vol. 2. (c) Fréchet, J. M. J. *Science* **1994**, *263*, 1710. (d) Ardoin, N.; Astruc, D. *Bull. Soc. Chim. Fr.* **1995**, 875. (e) Vögtle, F.; Issberner, J.; Moors, R. *Angew. Chem., Int. Ed. Engl.* **1994**, *33*, 2413. (f) Young, J. K.; Moore, J. S. *In Modern Acetylene−Chemistry*, Stang, P. J.; Diederich, F., Eds.; VCH: Weinheim, 1995; p 415. (g) Newkome, G. R.; Moorefield, C. N.; Vögtle, F. *Dendritic Molecules*; VCH: Weinheim, 1996.

(2) (a) *New Macromolecular Architectures and Supramolecular Polymers, Macromolecular Symposium*; Percec, V., Tirrell, D. A., Eds.; 1994; Vol. 77. (b) Percec, V.; Lando, J. *Polymers, Materials for the 21st Century, Macromolecular Symposium*; 1995; Vol. 98.

(3) (a) Gitsov, I.; Fréchet, J. M. J. *J. Am. Chem. Soc.* **1996**, *118*, 3785. (b) van Hest, J. C. M.; Delnoye, D. A. P.; Baars, M. W. P. L.; van Genderen, M. H. P.; Meijer, E. W. *Science* **1995**, *268*, 1596. (c) Zhou, Y.; Bruening, M. L.; Bergbreiter, D. E.; Crooks, R. M.; Wells, M. *J. Am. Chem. Soc.* **1996**, *118*, 3773. (d) Sadamoto, R.; Tomioka, N.; Aida, T. *J. Am. Chem. Soc.* **1996**, *118*, 3978.

(4) (a) Hawker, C. J.; Fréchet, J. M. J. *J. Am. Chem. Soc.* **1990**, *112*, 7638. (b) For a review, see: Hawker, C. J.; Wooley, K. L. In *Advances in Dendritic Macromolecules*; Newkome, G. R., Ed.; JAI Press: Greenwhich, 1995; Vol. 2, p 1.

(5) (a) Fréchet, J. M. J.; Henmi, M.; Gitsov, I.; Aoshima, S.; Ledue, M. R.; Grubbs, R. B. *Science* **1995**, *269*, 1080. (b) Hawker, C. J.; Fréchet, J. M. J.; Grubbs, R. B.; Dao, J. *J. Am. Chem. Soc.* **1995**, *117*, 10763. (c) Kawaguchi, T.; Walker, K. L.; Wilkins, C. L.; Moore, J. S. *J. Am. Chem. Soc.* **1995**, *117*, 2159. (d) Zeng, F.; Zimmerman, S. C. *J. Am. Chem. Soc.* **1996**, *118*, 5326.

(6) (a) Constable, E. C.; Harverson, P. *Chem. Commun.* **1996**, 33. (b) Huck, W. T. S.; van Veggel, F. C. J. M.; Kropman, B. L.; Blank, D. M. A.; Keim, E. G.; Smithers, M. M. A.; Reinhoudt, D. N. *J. Am. Chem. Soc.* **1995**, *117*, 8293. (c) Newkome, G. R.; Güther, R.; Moorefield, C. N.; Cardullo, F.; Echegoyen, L.; Pérez-Cordero, E.; Luftmann, H. *Angew. Chem. Int. Ed. Engl.* **1995**, *34*, 2023. (d) Amabilino, D. B.; Ashton, P. R.; Belohradsky, M.; Raymo, F. M.; Stoddart, J. F. *J. Chem. Soc. Chem. Commun.* **1995**, 751. (e) Zimmerman, S. C.; Zeng, F.; Reichert, D. E. C.; Kolotuchin, S. V. *Science* **1996**, *271*, 1095.

S0002-7863(96)03295-7 CCC: $14.00 © 1997 American Chemical Society

Scheme 1. Schematic Representation of (a) the Self-Assembly of **12-ABG** into a Supramolecular Cylindrical Dendrimer and the Subsequent Formation of the Columnar Hexagonal LC Supramolecular Assembly and (b) the Self-Assembly of **12G2-AG** into a Spherical Supramolecular Dendrimer and the Subsequent Formation of the Cubic LC Supramolecular Assembly

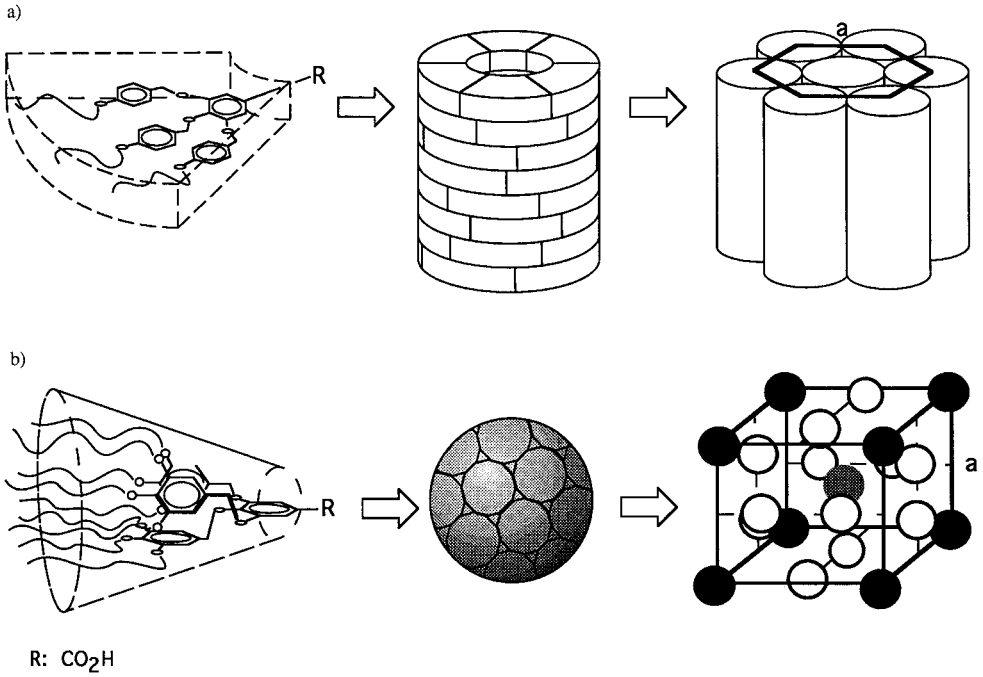

We are elaborating synthetic strategies which provide a molecular engineering approach to monodendrons and both macromolecular and supramolecular dendrimers which exhibit a predictable well defined shape in crystalline, ordered and disordered melt (i.e., liquid-crystalline and isotropic liquid) states. This shape is responsible for the formation of an ordered LC or crystalline assembly which is analyzed by X-ray diffraction techniques and generates direct information on the shape and size of the dendrimers and of their internal order.[9,10] Cylindrical dendrimers are systematically obtained by polymerization or self-assembly of monodendrons which exhibit a tapered fan shape.[10] In conformity with the same hypothesis, cone-shaped monodendrons should produce *via* similar techniques spherical dendrimers.

Scheme 1 outlines the strategy developed in our laboratory for the rational design of monodendrons which exhibit respectively flat tapered and conical shapes. Flat tapered monodendrons are produced from 3,4,5-tris(4-**a**lkyl-1-oxy)**b**enzyloxybenzoate (**12-ABG** where **G** stands for **g**allate) building blocks (Scheme 1a), while 3,4,5-tris[3,4,5-tris(alkyl-1-oxy)benzyloxy]-benzoate units should favor the generation of a conical shape (Scheme 1b). Molecular modeling of the monodendrons from Scheme 1 demonstrated that monosubstitution of their external benzyl ethers with alkyl groups only in the 4-position permits their independent free rotation about the benzyl ether bond. Consequently, these monodendrons can be fitted into a flat tapered shape (Scheme 1a). Substitution of the same benzyl ethers with alkyl groups in their 3,4,5-positions (Scheme 1b) allows only a restricted-cooperative rotation which requires the two external benzyl ethers to be approximately orthogonal to the internal one. This cooperative rotation favors a conical shaped monodendron. In addition, these architectural differences also produce a different curvature on the external surface of the corresponding monodendron. Interfacial curvature plays an important role in the formation of lyotropic and related thermotropic LC phases.[11−18] A detailed discussion of the geometrical aspects of lyotropic LC phases which supports the

(7) (a) Tomalia, D. A.; Baker, H.; Dewald, J.; Hall, M.; Kallos, G.; Martin, S.; Ryder, J.; Smith, P. *Macromolecules* **1996**, *19*, 2466. (b) Newkome, G. R,; Yao, Z.; Baker, G. R.; Gupta, V. K.; Russo, P. S.; Saunders, M. J. *J. Am. Chem. Soc.* **1986**, *108*, 849. (c) Newkome, G. R.; Moorefield, C. N.; Baker, G. R.; Behera, R. K.; Escamilla, G. H.; Saunders, M. J. *Angew. Chem., Int. Ed. Engl.* **1992**, *31*, 917. (d) Hawker, C. J.; Farrington, P. J.; MacKay, M. E.; Wooley, K. L.; Fréchet, J. M. J. *J. Am. Chem. Soc.* **1995**, *117*, 4409. (e) Sheiko, S. S.; Eckert, G.; Ignat'eva, G.; Muzafarov, A. M.; Spickermann, J.; Räder, H. J.; Möller, M. *Macromol. Rapid Commun.* **1996**, *17*, 283. (f) Saville, P. M.; Reynolds, P. A.; White, J. W.; Hawker, C. J.; Fréchet, J. M. J.; Wooley, K. L.; Penfold, J.; Webster, J. R. P. *J. Phys. Chem.* **1995**, *99*, 8283.

(8) Tomalia, D. A. in ref 1a, p 229 and personal communication.

(9) (a) Percec, V.; Chu, P.; Ungar, G.; Zhou, J. *J. Am. Chem. Soc.* **1995**, *117*, 11441. (b) Percec, V. *Pure Appl. Chem.* **1995**, *67*, 2031.

(10) Percec, V.; Johansson, G.; Heck, J.; Ungar, G.; Batty, S. V. *J. Chem. Soc. Perkins Trans. 1* **1993**, 1411. (b) Percec, V.; Heck, J.; Tomazos, D.; Falkenberg, F.; Blackwell, H.; Ungar, G. *J. Chem. Soc., Perkin Trans. 1* **1993**, 2799. (c) Percec, V.; Heck, J. A.; Tomazos, D.; Ungar, G. *J. Chem. Soc., Perkin Trans. 2* **1993**, 2381. (d) Johansson, G.; Percec, V.; Ungar, G.; Abramic, D. *J. Chem. Soc., Perkin Trans. 1*, **1994**, 447. (e) Percec, V. Tomazos, D.; Heck, J.; Blackwell, H.; Ungar, G. *J. Chem. Soc., Perkin Trans. 2* **1994**, 31. (f) Percec, V.; Schlueter, D.; Kwon, Y. K.; Blackwell, J.; Möller, M.; Slangen, P. J. *Macromolecules* **1995**, *28*, 8807. (g) Kwon, Y. K.; Chvalun, S. N.; Blackwell, J.; Percec, V.; Heck, J. A. *Macromolecules*, **1995**, *28*, 1552 and references therein. (h) Percec, V.; Johansson, G.; Ungar, G.; Zhou, J. *J. Am. Chem. Soc.* **1996**, *41*, 9855. (i) For a brief review, see: Percec, V.; Johansson, G; Schlueter, D.; Ronda, J. C.; Ungar, G. *Macromol. Symp.* **1996**, *101*, 43.

(11) (a) Tiddy, G. J. T. *Phys. Rep.* **1980**, *57*, 1. (b) Small, D. M. *Handbook of Lipid Research*; Plenum Press: New York, 1986. (c) Degiorgio, V.; Corti, M. *Physics of Amphiphiles: Micelles, Vesicles and Microemulsions*; North-Holland: Amsterdam, 1985. (d) Laughlin, R. G. *The Aqueous Phase Behavior of Surfactants*; Academic Press: San Diego, 1994. (e) Hoffmann, H. *Adv. Colloid. Interface. Sci.* **1990**, *32*, 123. (f) Ringsdorf, H.; Schlarb, B.; Venzmer, J. *Angew. Chem., Int. Ed. Engl.* **1988**, *27*, 113. (g) Lasic, D. D. *Angew. Chem., Int. Ed. Engl.* **1994**, *33*, 1685.

(12) Thomas, E. L.; Anderson, P. M.; Henkee, C. S.; Hoffman, D. *Nature* **1988**, *334*, 598.

(13) Hillmyer, M. A.; Bates, F. S.; Almdal, K.; Mortensen, K.; Ryan, A. J.; Fairclough, J. P. A. *Science* **1996**, *271*, 976 and references cited therein.

(14) (a) Sadoc, J. F.; Charvolin, J., *J. Phys. France* **1986**, *47*, 683. (b) Israelachvili, J. *Intermolecular and Surface Forces*, 2nd ed.; Academic Press: London, 1992. (c) For the only series of systematic investigations on the effect of molecular geometry of surfactants on their lyotropic LC phase, see: Kratzat, K.; Finkelmann, H. J. *Colloid. Interface Sci.* **1996**, *181*, 542 and references cited therein.

(15) (a) Gruner, S. M. *J. Phys. Chem.* **1989**, *93*, 7562. (b) Tate, M. W.; Eikenberry, E. F.; Turner, D. C.; Shyamsunder, E.; Gruner, S. M. *Chem. Phys. Lip.* **1991**, *57*, 147.

Scheme 2. Synthesis of **3,4,5-*t*-12Gn-AG-CH3** and **3,4,5-*t*-12Gn-AG-CH_2OH**

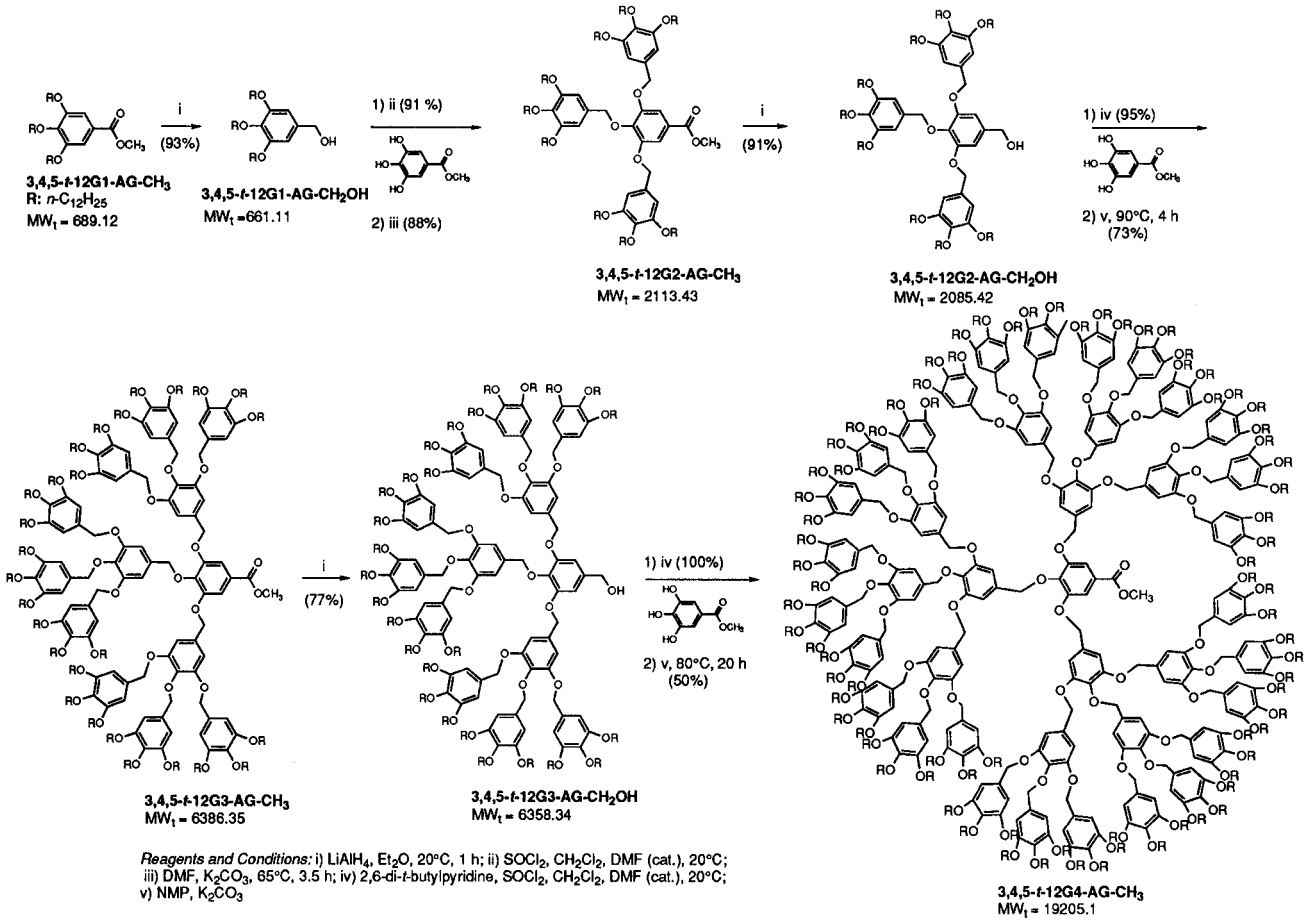

rationalization of the molecular design and the observed phase behavior of the monodendrons reported in this publication is available in the Supporting Information.[14−29] In contrast to the abundance and biological significance of lyotropic systems which exhibit cubic symmetry[15b,18,19,20] relatively few thermotropic systems which display similar phases[21−29] are known.

This publication reports the rational design, synthesis, and characterization of the first four generations of monodendrons which, as a function of generation number, exhibit conical and respectively hemispherical shapes. These monodendrons self-assemble into supramolecular dendrimers which display a spherical shape that generates a novel thermotropic cubic LC phase which was analyzed by X-ray diffraction and provided the first confirmation and quantitative characterization of the widely suspected spherical shape of dendrimers in an ordered melt state.

Results and Discussion

Synthesis of Monodendrons. Our approach to the synthesis of benzyl ether type monodendrons is based on the use of a polyhydroxy methyl benzoate building block. The size and shape of the monodendron at each generation is determined by the number (1, 2, or 3) and position (3,4-, 3,5- or 3,4,5-) of the reactive hydroxyl groups of the methyl benzoate. Nucleophilic substitution of the hydroxylic groups of polyhydroxy methylbenzoate with an appropriate electrophile determines the surface functionality (**R** in Scheme 2) of the monodendron. In this investigation we used the AB_3 monomer methyl 3,4,5-trihydroxybenzoate (methyl gallate) and its first generation monodendron, methyl 3,4,5-tris(*n*-dodecyloxy)benzoate (**3,4,5-*t*-12G1-AG-CH_3**) where 3,4,5- refers to the position of the alkyloxy tails of the methylbenzoate (*i.e.*, methyl gallate is **AG-CH_3**) ring and ***t*** to the number of alkyl tails (***t*** = tris, ***b*** = bis, ***m*** = mono). The prefix **3,4,5-*t*-** will no longer be referred to in this discussion as it remains consistent throughout. The number preceding the letter **G** (from gallate) refers to the number of carbon atoms in the linear alkyl tails, while the number following **G** refers to the generation number.

Scheme 2 outlines the convergent[4] stepwise synthesis of the second (G2), third (G3), and fourth (G4) generation monoden-

(16) (a) Scriven, L. E. *Nature* **1976**, *263*, 123. (b) Sadoc, J. F.; Charvolin, J. *Acta Crystallogr.* A *45*, 10.
(17) (a) Fontell, K.; Fox, K. K.; Hansson, E. *Mol. Cryst. Liq. Cryst., Lett.* **1985**, *1*, 9. (b) Charvolin, J.; Sadoc, J. F.; *J. Phys. France* **1988**, *49*, 521. (c) Vargas, R.; Mariani, P.; Gulik, A.; Luzzati, V. *J. Mol. Biol.* **1992**, *225*, 137. (d) Luzzati, V.; Vargas, R.; Mariani, P.; Gulik, A.; Delacroix, H. *J. Mol. Biol.* **1993**, *229*, 540.
(18) (a) Mariani, P.; Luzzati, V.; Delacroix, H. *J. Mol. Biol.* **1988**, *204*, 165. (b) Seddon, J. M. *Biochemistry* **1990**, *29*, 7997.
(19) (a) Luzzati, V.; Spegt, P. A. *Nature* **1967**, *215*, 701. (b) Luzzati, V.; Gulik-Krzywicki, T.; Tardieu, A. *Nature* **1968**, *218*, 1031.
(20) Seddon, J. M.; Templer, R. H. *Phil. Trans. R. Soc. Lond. A* **1993**, *344*, 377.
(21) Tardieu, A.; Billard, J. *J. Phys. France* **1976**, *37 C3*, 79.
(22) Etherington, G.; Leadbetter, A. J.; Wang, X. J.; Gray, G. W.; Tajbakhsh, A. R. *Liq. Cryst.* **1986**, *1*, 209. Leadbetter, A. J. In *Thermotropic Liquid Crystals*, Gray, G. W., Ed.; J. Wiley: New York, 1987; p 1.
(23) Charvolin, J.; Sadoc, J. F. *J. Phys. France* **1987**, *48*, 1559.
(24) Bruce, D. W.; Donnio, B.; Hudson, S. A.; Levelut, A. M.; Megtert, S.; Petermann, D.; Veber, M. *J. Phys. II (France)* **1995**, *5*, 289.
(25) Fischer, S.; Fischer, H.; Diele, S.; Pelzl, G.; Jankowski, K.; Schmidt, R. R.; Vill, V. *Liq. Cryst.* **1994**, *6*, 855.
(26) Latterman, G.; Staufer, G. *Mol. Cryst. Liq. Cryst.* **1990**, *191*, 199.
(27) Ungar, G.; Percec, V.; Heck, J. *Thermotropic cubic, smectic and columnar phases in a class of side-chain polymers*; 15th International Liquid Crystal Conference, Budapest, 3−8 July 1994; in preparation.
(28) Borisch, K.; Diele, S.; Goering, P.; Tschierske, C. *Chem. Commun.* **1996**, 237.
(29) Chandrasekhar, S.; Shadashiva, B. K.; Suresh, K. A. *Pramana* **1977**, *9*, 471.

Table 1. Theoretical and Experimental Molecular Weights Determined by MALDI-TOF MS and GPC and Thermal Transitions of Monodendrons **12Gn-AG-CH_3**, **12Gn-AG-CH_2OH**, and **12Gn-AG**[c]

monodendron	MW_t	*m/z* [M + Na^+] (MALDI-TOF)	M_n (GPC)	M_w/M_n (GPC)	M_n/MW_t	thermal transitions (°C) and corresponding enthalpy changes (kcal/mol) heating	cooling
12G1-AG-CH_3	689.12		910	1.04	1.32	k 44 (23.2) i k 23 (15.9) i	i 4 (15.5) k
12G2-AG-CH_3	2113.4	2136.1	2448	1.07	1.16	k 57 (37.0) i k 10 (−5.49) k 57 (36.7) i	i 35 (0.74) Cu 11, 4 (21.9)[a] k
12G3-AG-CH_3	6386.4	6410.7	5872	1.11	0.92	k −13 (22.7) k 39 (8.43) Cu 94 (1.22)i k −11 (29.2) Cu 94 (1.22) i	i 75 (0.81) Cu 47 (0.85) k −16 (28.0) k
12G4-AG-CH_3	19205.1	19228.5	11871	1.08	0.62	k −13 (68.7) g 37 Cu 77 i[b] k −11 (88.3) g 42 Cu 77 i[b]	i 61[b] Cu 47 g −17 (76.9) k
12G1-AG-CH_2OH	661.11		897	1.03	1.36	k 50 (19.7) i k 47 (12.7) i	i 37 (11.7) k
12G2-AG-CH_2OH	2085.4	2108.4	2495	1.04	1.20	k 36 (4.31) k 59 (27.4) Cu 88 (1.12) i k −8 (7.02) k 38 (−3.18) k 58 (4.96) Cu 88 (0.87) i	i 80 (0.68) Cu −15 (23.3) k
12G3-AG-CH_2OH	6358.3	6381.5	5914	1.08	0.93	k −12 (25.0) k 45 (1.84) Cu 107 (1.35) i k −12 (30.6) Cu 106 (1.22) i	i 93 (0.90) Cu −17 (25.6) k
12G1-AG	675.10		934	1.06	1.38	k 60 (14.9) i k 59 (14.3) i	i 33 (14.1) k
12G2-AG	2099.4	2122.8	2632	1.04	1.25	k 85 (25.6) Cu 119 (1.27) i k −9 (5.62) k 43 (−19.5) k 83 (24.3) Cu 117 (0.96) i	i 111 (0.87) Cu −15 (8.67) k
12G3-AG	6372.3	6395.3	5749	1.13	0.90	k −15 (31.5) Cu 140 (1.63) i k −12 (29.7) Cu 139 (1.17) i	i 127 (1.17) Cu −17 (31.0) k
12G4-AG	19191.3	19214.8	11274	1.11	0.59	k −14 (83.3) Cu 85 i[b] k −12 (105.9) Cu 85 i[b]	i 72 Cu −18 (89.4) k

[a] Sum of enthalpies from overlapped peaks. [b] Observed by optical polarized microscopy. [c] Data from the first heating and cooling scans are on the first line, and data from the second heating are on the second line.

drons, **12Gn-AG-CH_3**. The ester group of the first generation monodendron, **12G1-AG-CH_3**, was reduced with $LiAlH_4$ to give the crystalline benzyl alcohol, **12G1-AG-CH_2OH**, in 93% yield. Its quantitative chlorination with $SOCl_2$ and a catalytic amount of DMF produced the benzyl chloride, **12G1-AG-CH_2Cl**, in 91% yield. This compound was isolated by aqueous workup followed by recrystallization from acetone. However, in subsequent generations the benzyl chlorides were used without further purification.

Previous work in our[10] and other[30] laboratories demonstrated the quantitative alkylation of methyl gallate with 3.0 equiv of *p*-(*n*-dodecyloxy)benzyl chloride by using K_2CO_3 as base in DMF (65−80 °C, 4−8 h) to generate methyl 3,4,5-tris[*p*-(*n*-dodecyloxy)benzyloxy]benzoate in >90% isolated yields. Under similar conditions, complete alkylation of methyl gallate with **12G1-AG-CH_2Cl** was accomplished in 3.5 h at 65 °C to give the second generation monodendron, **12G2-AG-CH_3**, in 88% yield after purification by column chromatography (b. Al_2O_3, CH_2Cl_2). The complete consumption of **12G1-AG-CH_2Cl** was monitored by the disappearance of the benzylic $-CH_2-$ protons at 4.47 ppm in the ^1H NMR spectrum. Quantitative reduction of **12G2-AG-CH_3** with $LiAlH_4$ produced **12G2-AG-CH_2OH** in 91% yield after recrystallization from acetone.

Fréchet *et al.*[4a] have described the mild bromination of the benzylic alcohol moiety of AB_2 dendritic wedges with CBr_4/PPh_3. While this method proceeds quantitatively in the absence of side reactions, it suffers from the generation of stoichiometric amounts of triphenylphosphine oxide byproducts. At higher generation number, the reaction is considerably slower and requires an excess of reagents. $SOCl_2$ is the most attractive reagent for the chlorination of benzyl alcohols due to the short reaction time, low temperature, low price, and ease of manipulation. In addition, under our reaction conditions, the reactivity of benzyl chloride is sufficient to produce a quantitative etherification. The chlorination of **12Gn-AG-CH_2OH** ($n > 1$) with $SOCl_2$ in the presence of a catalytic amount of DMF was completed within 5−10 min at room temperature. However, within a few minutes (for **12Gn-AG-CH_2Cl**) to several hours (for **12G2-AG-CH_2Cl**), the HCl induced cleavage of the highly activated *p*-alkoxybenzyl ether moieties was observed in the ^1H NMR spectrum. An excess of Et_3N or other similar organic bases retarded the decomposition but did not completely suppress it. When the chlorination was carried out in the presence of an excess of the non-nucleophilic base scavenger, 2,6-di-*tert*-butylpyridine, which is known to be an extremely eficient proton-trap,[31] no decomposition products were observed even after several days in solution or months in solid state. Optimization of the reaction conditions revealed that the chlorination proceeded equally well when a stoichiometric amount of 2,6-di-*tert*-butylpyridine was used. The chlorinated product could be used after aqueous workup in the next step without further purification.

The alkylation of methyl gallate with **12G2-AG-CH_2Cl** was carried out in NMP at 80 °C due to the limited solubility in DMF of the starting benzyl chloride. At 80 °C in DMF, the insoluble benzyl chloride melted, and the interfacial reaction proceeded smoothly with vigorous stirring. Purification by column chromatography (b. Al_2O_3, hexanes) produced **12G3-AG-CH_3** in 73% yield. After reduction with $LiAlH_4$, chlorination with $SOCl_2$/di-*tert*-butylpyridine and alkylation of methyl gallate, **12G4-AG-CH_3**, was obtained in 33% overall yield from **12G3-AG-CH_3**. **12G3-AG-CH_2OH** and **12G4-AG-CH_3** were purified by column chromatography (b. Al_2O_3). The final alkylation step required a reaction time of 20 h in NMP at 80 °C. The extent of this reaction was monitored by a combination of ^1H NMR and GPC analysis.

Monodendrons with a carboxylic acid functionality at their focal point were prepared by basic hydrolysis of the corresponding esters, **12Gn-AG-CH_3**. The products, **12Gn-AG**, were obtained after protonation in THF solution with 50% aqueous acetic or formic acid.

Structural Characterization of Monodendrons. The purity of all monodendrons was determined by a combination of TLC, GPC, HPLC, ^1H NMR and $^{13}C\{^1H\}$ NMR spectroscopy, elemental analysis, and MALDI-TOF mass spectrometry. Table

(30) Mâlthete, J.; Nguyen, H. T.; Levelut, A. M. *J. Chem. Soc. Chem. Commun.* **1986**, 1548.

(31) Brown, H. C.; Kanner, B. *J. Am. Chem. Soc.* **1953**, *75*, 3865.

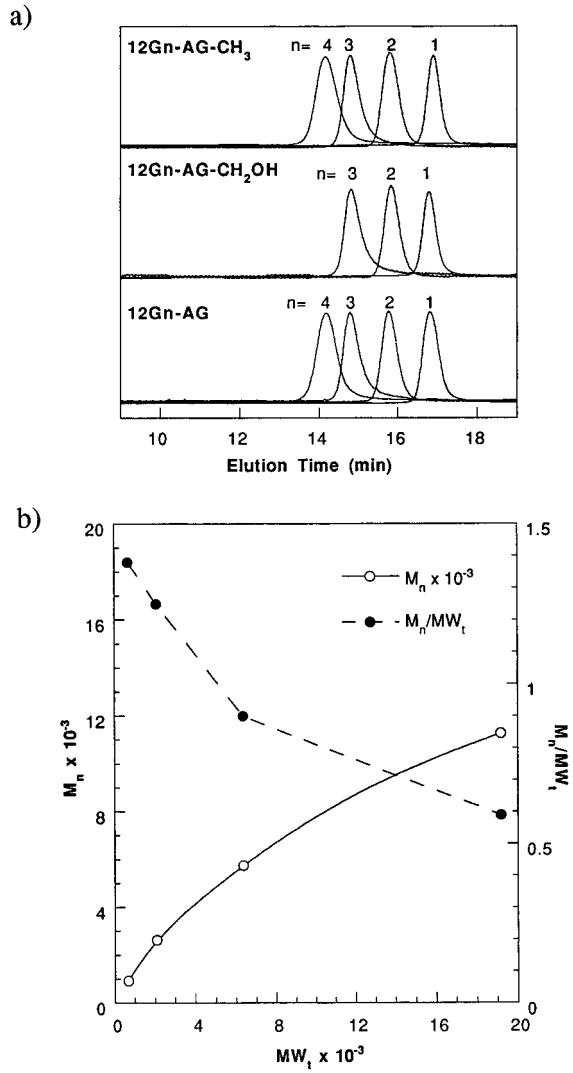

Figure 1. (a) GPC traces of **12Gn-AG-CH$_3$**, **12Gn-AG-CH$_2$OH**, and **12Gn-AG** (n = 1−4). (b) Dependence of M_n (○) and the ratio, M_n/MW$_t$ (●), *vs.* theoretical molecular weight (MW$_t$) of **12Gn-AG** (n = 1−4).

1 summarizes the theoretical molecular weights (MW$_t$), the absolute molecular weights determined by MALDI-TOF MS, relative number-average molecular weight (M_n) determined by GPC with polystyrene standards, and the ratio M_n/MW$_t$ for **12Gn-AG-CH$_3$**, **12Gn-AG-CH$_2$OH**, and **12Gn-AG**. The corresponding GPC traces are shown in Figure 1a. All monodendrons are monodisperse and show monomodal molecular weight distribution. The large increase (>3-fold) in molecular weight with generation number guarantees excellent resolution of lower molecular weight fragments arising from incomplete alkylation reactions. These fragments are not observed in the GPC/HPLC traces from Figure 1a.

MALDI-TOF mass spectra of **12Gn-AG-CH$_3$**, with n = 2, 3 and 4, **12Gn-AG-CH$_2$OH**, with n = 2 and 3, and **12Gn-AG**, with n = 2, 3, and 4, gave the correct molecular peak (Table 1 and Supporting Information). Lower mass fragments which do not correspond to intermediary compounds were observed in small amounts in several cases of low generations monodendrons. Their origin will be discussed in a full report on the MALDI-TOF MS characterization of these and other monodendrons and dendrimers.

Figure 1b plots the dependence of the M_n of **12Gn-AG** determined by GPC on its MW$_t$. M_n increases nonlinearly with the increase in absolute molecular weight, MW$_t$. At higher MW$_t$, the slope of the M_n dependence decreases continuously. These results are a consequence of the by now well-accepted tendency of dendrimers and high generation monodendrons to exhibit a lower hydrodynamic volume than their linear homologues due to their compact architecture.[4a,32] The same plot shows the dependence of M_n/MW$_t$ on MW$_t$. The AB$_3$ nature of the repeat unit of the monodendrons results in the formation of very compact monodendron structures at the third and fourth generation.

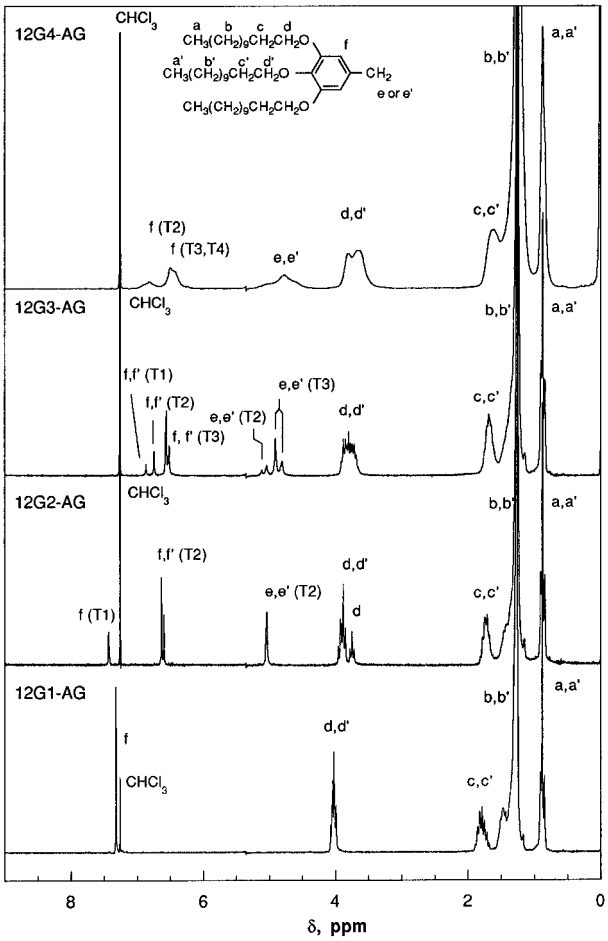

Figure 2. 200 MHz ^{1}H NMR spectra of **12Gn-AG** (n = 1−4) ($CDCl_3$, TMS, 20 °C).

NMR Analysis. The reaction sequence (a) $LiAlH_4$ reduction, (b) $SOCl_2$ chlorination, and (c) alkylation for each generation was quantitatively monitored by observation of the formation and consumption of benzylic C*H*$_2$OH and C*H*$_2$Cl protons. Regardless of the generation number, the benzylic C*H*$_2$OH protons were observed as an easily distinguishable doublet shifted about 0.1 ppm downfield from the benzylic C*H*$_2$Cl protons. During the transformation from **12G3-AG-CH$_2$Cl** to **12G4-AG-CH$_3$**, the signal arising from C*H*$_2$Cl was somewhat broadened and of low sensitivity; therefore, GPC analysis was used as a complementary technique. The combination of ^{1}H and ^{13}C{^{1}H} NMR techniques was used to verify the structural purity of the monodendrons as well.

Figure 2 shows the ^{1}H NMR spectra of the series of carboxylic acid functionalized monodendrons, **12Gn-AG**. The chemical structure of the outermost tier of the monodendron is also drawn with the protons labeled H$_a$-H$_f$. The central benzene unit of each monodendron is defined as tier 1 (T1), and at each generation a new tier (Tn) is formed with three times larger

(32) Tomalia, D. A.; Naylor, A. M.; Goddard, W. A., III *Angew. Chem., Int. Ed. Engl.* **1990**, *29*, 138.

number of benzene rings than in the previous tier. The aromatic protons are labeled H_f, and the benzylic protons on position 1 of the aromatic ring are labeled H_e. The position of an aromatic or benzylic proton within the monodendritic structure can be pinpointed by the tier to which it belongs and its attachment to the oxygen atom (*meta* or *para*) of the aromatic ring from the previous tier. The former is indicated in parentheses (T1, T2, T3, or T4). Resonances arising from substitution in the *para* position are distinguished from *meta* substituents by a prime (′) superscript. The methylenic protons of the alkyl tails are always located on the periphery of the monodendron, and, therefore, only their *meta* or *para* substitution pattern is specified. With increasing generation number, the ^{1}H NMR signals of **12Gn-AG** begin to broaden significantly, and nearly all resolution is lost in the spectrum of **12G4-AG**. The broad signals of **12G4-AG** are attributed to the extremely dense packed structure of the monodendron arising from the AB_3 substitution pattern and the high alkyl tail density generated at the periphery. As a consequence, internal conformational mobility is reduced to such an extent on the NMR time scale that broadened signals arise from the individual contributions of all available conformations.

The ^{1}H NMR spectrum of the third generation monodendron **12G3-AG** contains the most accessible information, since the effect of the dense packing within the dendritic structure can be rationalized by the identification of the well-resolved NMR signals arising from protons on three different tiers. From the assignments in Figure 2 we concluded that the aromatic and benzylic protons near the periphery (T3) of the monodendron are shifted to higher field. An opposite behavior has been observed in other monodendrons.[4a]

The ^{13}C{^{1}H} NMR spectra of **12Gn-AG**, shown in Figure 3, were used to confirm the ^{1}H-NMR assignments. The aromatic carbons are labeled C-1, C-2, C-3, or C-4 based on their ring position. The benzylic carbons are labeled H_h and $H_{h'}$ based on *meta*- and *para*-attachment as described previously. The spectrum of **12G3-AG** displays strong signals from C-2 at 105.8, 107.2, and 110.0 ppm. They were assigned to C-2 of T3, T2, and T1, respectively, based on their expected decrease in signal intensity. The aromatic carbons at the periphery (T3) are shifted 1.4 ppm upfield of the internal T2 carbons and are therefore shielded. This shielding is due to the through-space interaction of the C-2 nucleus with the anisotropic shielding zone of the adjacent aromatic rings in the densely packed monodendron. Inspection of C-1, C-3, and C-4 of **12G3-AG** supports this conclusion. The carbons from T1 are neglected due to the susceptibility of their chemical shifts to electronic effects arising from their attachment to the carboxylic acid functionalized aromatic ring. Carbons C-1 and C-4 are further from the anisotropic shielding zone of the adjacent aromatic rings and show a difference of only 0.4 ppm in their chemical shifts from T3 and T2. C-3 shows only one strong peak corresponding to the overlapped resonances from all of the C-3 protons, regardless of which tier they belong to. Any shielding of the peripheral C-3 carbons is negated by the electronic effects arising from the vicinal oxygen atom. This shielding effect is a consequence of the cone-shaped geometry of the monodendritic *exo*-receptor and can be understood by inspecting the ^{1}H NMR spectrum of **12G2-AG** and of several model compounds. A detailed discussion is available in the Supporting Information.

Molecular models of the top and side views of **12G2-AG** are shown in Figure 4. The flanking aromatic rings are rotated around their $C_{Ar}-CH_2$ bonds and situated orthogonal to the central aromatic ring. Free rotation of the benzyl ether groups in **12Gn-AG** is allowed only in a cooperative way which

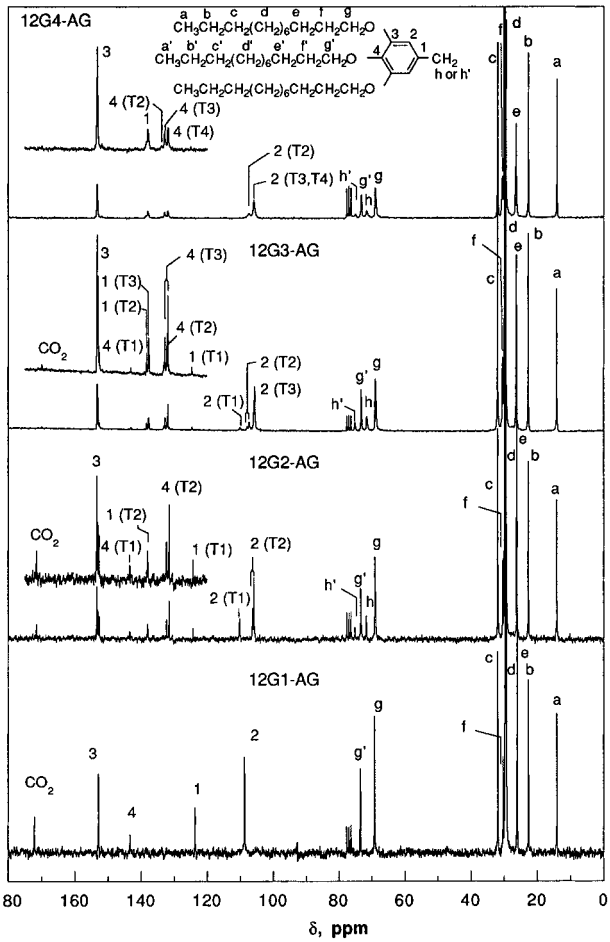

Figure 3. 50 MHz ^{13}C{^{1}H} NMR spectra of **12Gn-AG** ($n = 1-4$) ($CDCl_3$, 20 °C).

requires the relative orthogonal arrangement mentioned above. In the case of **12ABG** free random rotation of the three benzyl ethers is allowed. The cooperative rotation of the benzyl ether groups of the **12Gn-AG** is dictated by the presence of the two alkyloxy groups in the 3,5 positions of the **12G1-AG**. The methylenic protons, $H_{e''}$ (from Figure 2 of Supporting Information), are situated within 4−5 Å of the nuclei of the flanking aromatic rings. The side view dramatizes the cone shape of this monodendron (Scheme 1, Figure 4).

Thermal Analysis. The phase behavior of the monodendrons **12Gn-AG-CH$_3$**, **12Gn-AG-CH$_2$OH**, and **12Gn-AG** was characterized by a combination of thermal optical polarized microscopy and differential scanning calorimetry (DSC). This phase was assigned based on X-ray analysis, and its structure will be described in detail in the next section. A detailed discussion of the DSC traces is presented in the Supporting Information. The phase behavior of **12Gn-AG** is summarized in Table 1. **12Gn-AG-CH$_2$OH** with $n = 2$ and 3 and **12Gn-AG-CH$_3$** with $n = 3$ and 4 display an enantiotropic cubic LC phase, while **12G2-AG-CH$_3$** shows only a monotropic cubic phase. **12G1-AG-CH$_3$** and **12G1-AG** are only crystalline. On the optical polarized microscope the cubic phase is as expected optically isotropic.

Determination of the Shape and Size of the Supramolecular Dendrimers by X-ray Analysis of Their Cubic LC Phase. Only a diffuse ring with a maximum corresponding to a Bragg spacing of 4.7 Å was observed in the wide-angle region for the cubic phase of all compounds. A considerable number of sharp low-angle reflections were recorded for monodendrons **12G2-AG** and **12G3-AG**. The low-angle powder diffractogram of **12G2-AG** in the cubic phase is shown in Figure 4a of

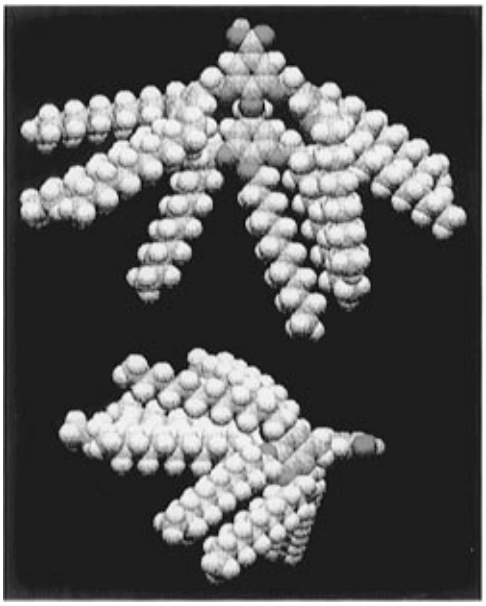

Figure 4. Molecular models of **12G2-AG**. Top: front view, bottom: side view.

Table 2. Measured (d_{exp}) and Calculated (d_{calc}) *d*-Spacings and Integrated Intensities (*I*) (Lorentz and Multiplicity Corrected) of the Cubic Phase Generated by **12Gn-AG**

reflection	**12G2-AG** at 105 °C d_{exp} (Å)/ d_{calc} (Å)/*I*	**12G3-AG** at 80 °C d_{exp} (Å)/ d_{calc} (Å)/*I*	**12G4-AG** at 20 °C d_{exp} (Å)/ d_{calc} (Å)/*I*
100			
110	48.76/48.29/0.05	56.1/56.00/0.05	
111			
200	34.54/34.15/100	39.48/39.60/73	41.90/42.00/94
210	30.93/30.54/80	35.40/35.42/100	37.70/37.57/100
211	28.28/27.88/66	32.64/32.33/55	34.30/34.29/32
220	23.74/24.15/0.7	28.05/28.00/0.5	
221/300			
310	21.29/21.60/0.1	29.40/25.05/0.4	
311			
222			
320		22.08/21.97/0.3	
321	18.19/18.25/0.8	21.09/21.17/0.5	
400	17.00/17.08/3.5	19.87/19.80/1.3	

Supporting Information, and the list of observed and calculated *d*-spacings is given in Table 2. In contrast, **12G4-AG** gave no sharp reflections unless it was cooled slowly (1 °C/h) from the isotropic phase. Even in the latter case it gave only three reflections which corresponded closely to the strongest reflections observed in **12G2-AG** and **12G3-AG**. The reflections from **12G2-AG** and **12G3-AG**, whose reciprocal *d*-spacings were in the ratio $\sqrt{2}:\sqrt{4}:\sqrt{5}:\sqrt{6}:\sqrt{8}:\sqrt{10}:\sqrt{13}:\sqrt{14}:\sqrt{16}$:..., could be indexed on the primitive cubic lattice ($a = 68.3$ Å for **12G2-AG** and $a = 79.2$ Å for **12G3-AG**) with the first reflection assigned the index (110) (Table 2). The three reflections of **12G4-AG** are indexed as (200), (210), and (211), giving the unit cell parameter $a = 84.0$ Å. In view of the similarity in the diffractograms from the G2, G3, and G4 compounds, their structure is regarded as isomorphous. The absence of higher order reflections in **12G4-AG** is attributed to its higher positional disorder.

Diffraction patterns from monodomains of **12G2-AG** recorded along a ⟨100⟩ direction (Figure 4b of Supporting Information) show the presence of reflections (410) and (420) which are not seen in the powder pattern. Reflection (300) is absent, in agreement with the powder pattern. Monodomain patterns recorded along ⟨110⟩ and ⟨210⟩ clearly demonstrate the absence of reflections (111), (113), and (221). The observed reflections satisfy the conditions for space groups $Pm\bar{3}n$ and $P\bar{4}3n$, namely, 00h: h = even and *hhl*: l = even. Hence, in accordance with convention, the space group with the highest symmetry, *viz.* $Pm\bar{3}n$, is chosen for the present cubic phase (the other space group does not possess a center of symmetry). An LC cubic phase with this symmetry is also known to form in some Type I lyotropic biological lipid systems.[17]

Reconstruction of Electron Density Maps. In order to resolve the structure of the cubic phase, we first calculated the electron density maps of the unit cell using the observed diffracted intensities. The correct choice of phase for individual reflections was reached by a process of elimination, assuming the tendency for phase separation between aromatic and aliphatic moieties, which is generally believed to be a primary cause of formation of most thermotropic layered, columnar and cubic phases.[33]

The volume fractions of the aromatic region (the core region of the molecule including the carboxylic group) and of the aliphatic region were obtained by computing the volume enclosed by the van der Waals surface of the respective regions of the molecule and assuming that the packing fractions are the same for the two regions. For compounds **12G2-AG**, **12G3-AG**, and **12G4-AG** the volume fractions occupied by the aromatic region are, respectively, 18, 19, and 20% of the total volume. The *electron* density of a given region is computed by summing the electrons contributed by each atom in the region and dividing the sum by the van der Waals volume. The same space-filling efficiency (packing coefficient) is assumed for both the aliphatic and aromatic regions. The electron density of the aromatic region estimated in this manner is 1.5 times that of the aliphatic region.

In terms of diffraction experiments, the electron density $\rho(\vec{r})$ in the cubic phase, as in any periodic structure, can be expressed as a Fourier series, the coefficients of which are the structure factors F_{hkl} corresponding to the individual reflections. In general

$$\rho(\vec{r}) - \rho_o = \sum_{h,k,l} \tilde{F}_{hkl} \exp[-i2\pi(hx + ky + lz)] \qquad (1)$$

Here ρ_0 is the average electron density and x, y, and z are the fractional coordinates of a point in the unit cell. $\tilde{F}$ denotes the generally complex structure factor which can be written as

$$\tilde{F}_{hkl} = |F_{hkl}| \exp(i\phi_{hkl}) \qquad (2)$$

Whereas the modulus $|F_{hkl}|$ is given by the square root of the intensity of the observed reflection, the phase ϕ_{hkl} is unknown. However, if the lattice is centrosymmetric, the structure factor becomes real, and the phase is restricted to only one of the two allowed values, 0 and π, thus making $F_{hkl} = \pm|F_{hkl}|$. The problem of our structure determination therefore essentially reduces to finding the correct sign, or phase, of F for each X-ray reflection.

For the specific case of $Pm\bar{3}n$ cubic symmetry eq 1 is reduced to the cosine series of the following form:

$$\rho(\vec{r}) - \rho_o = \sum_{h,k,l} F_{hkl} \cos(2\pi hx) \cos(2\pi ky) \cos(2\pi lz) \quad (1)$$

We start the X-ray analysis with the compound **12G4-AG** since its higher disorder in the cubic phase results in fewer

(33) (a) Skoulios, A.; Guillon, D. *Mol. Cryst. Liq. Cryst.* **1988**, *165*, 317. (b) Skoulios, A. *Makromol. Chem., Macromol. Symp.* **1992**, *62*, 201. (c) Ungar, G.; Abramic, D.; Percec, V.; Heck, J. A. *Liq. Cryst.* **1996**, *21*, 73. (d) Cistola, D. P.; Small, D. M. *J. Am. Chem. Soc.* **1990**, *112*, 3214.

Table 3. Characterization of Supramolecular Dendrimers Self-assembled from **12Gn-AG** Monodendrons

monodendron	density, d_{20} (g/cm^3)	T (°C)	cubic lattice dimension, a (Å)[b]	no. of monodendrons per unit cell, μ' [c]	no. of monodendrons per spherical dendrimer, μ[d]	distance from vacancies at positions d to centers of nearest dendrimer (Å)	distance from carboxylic hydrogen to the end of extended dodecyl chain (Å)
12G2-AG	0.99 (1.04)[a]	105	68.3 ± 0.4	90.0 (96)	11.3 (12.0)	24	26
12G3-AG	0.99 (1.04)[a]	80	79.2 ± 0.4	46.2 (48.0)	5.8 (6.0)	28	32
12G4-AG	0.99 (1.04)[a]	20	84.0 ± 0.3	15.2 (16.0)	1.9 (2.0)	30	37−38

[a] Assumed. [b] $a = (\sqrt{2}\cdot d_{110} + \sqrt{4}\cdot d_{200} + \sqrt{5}\cdot d_{210} + \sqrt{6}\cdot d_{211} + \sqrt{8}\cdot d_{220})/5$. [c] $\mu' = (a^3/d)/\mathrm{M}$. [d] $\mu = \mu'/8$.

observed diffraction lines, compared with **12G2-AG** and **12G3-AG**. Using the observed strong reflections ((200), (210), and (211), see Table 2), we have computed the electron density profiles in the cubic unit cell. The $2^3 = 8$ independent choices for the phases of these three reflections are reduced by half when the arbitrary choice of origin is allowed for. Out of the remaining four, two are related to the other two by inversion with respect to ρ_0.

In all three compounds studied these three reflections would capture the main coarse features of the electron density map. However, in compounds **12G2-AG** and **12G3-AG** the exclusion of higher reflections would mean an arbitrary truncation of the Fourier series. This would result in artefacts which could be rectified only by the inclusion of higher terms, with their correct sign, arising from all remaining reflections of reasonable intensity. In contrast, the "artifact" in the electron density distribution computed for **12G4-AG** is only in that the distribution would be smeared by averaging over a disordered lattice. If the disorder was thermal-like, the smearing could be taken account of by a Debye-Waller factor. While the electron density profile obtained from the diffractogram of **12G4-AG** will be more rounded than that of a typical individual unit cell, it will be basically correct, provided the correct phase choice for the three independent strong reflections is made. The profile resulting from such a naturally truncated series will then serve as a guide in selecting the correct phase choices for the larger number of reflections in the case of compounds **12G2-AG** and **12G3-AG**.

The electron density profiles have been computed for all four combinations of phases, namely "+ − ++", "++ − −", "− + − −" and "− − ++". The signs correspond to reflections (200), (210), (120), and (211), respectively.[34] The profiles are discussed further below. To help decide on the viability of a particular phase combination, electron density histograms were calculated for the above phase choices.

Electron Density Histograms. The histograms were obtained by dividing the unit cell into a large number (10^6) of small cells, counting the volume fraction of cells that have the electron density within a given interval (ρ, $\rho+\delta\rho$), and plotting these volume fractions against electron density. Such histograms have been used in the past.[18a] We use them to determine which combinations of structure factor phases give rise to good separation between the high- and low-density regions, while maintaining a volume ratio consistent with that calculated from the molecular model. In the ideal case of complete separation into two discrete phases we would expect the histogram corresponding to the correct phase choice to show a bimodal distribution of volume. However, there are two factors contributing toward broadening of the observed distribution: (1) the presence of disorder, *i.e.*, the averaging over fluctuations between individual cells resulting in apparent blurring of phase boundaries—see above and (2) genuine partial mixing of phases within individual unit cells.

As mentioned earlier, in the particular case of **12G4-AG**, model calculations show that the high electron density phase (aromatic region including the carboxylic group) occupies 20% of the volume, while the low-density aliphatic phase occupies the remaining 80%. In the ideal case we would thus expect the histogram to consist of two peaks, with a 20:80 ratio between the areas of the high-density and the low-density peak. Such a histogram would be an indication of the correct choice of the structure factor phase combination and, hence, of the underlying structural model. However, we expect a certain degree of smearing of the observed distributions due to the two factors outlined above.

Figure 5 shows electron density histograms, calculated from the intensity data for the cubic phase of **12G4-AG**, for the four distinguishable phase combinations. The dashed vertical line is the demarcation between the low density 80% and the high density 20% of the total volume. As is seen, the histogram for the phase combination "− + − −"(Figure 5c) is the inverse of the histogram for "+ − ++" (a), and similarly histogram "− − ++" (Figure 5d) is the inverse of histogram "++ − −" (Figure 5b). The "inverse" phase combinations "− + − −" and "− − ++" can be safely excluded at this stage since the demarcation line cuts through the peak of the histogram or near it, rather than through a trough. These distributions do not meet the expectation of a clean separation of aliphatic chains into an 80% volume fraction region of low and constant[33c] density. On the other hand, the histograms labeled "+ − ++" and "++ − −" show that both these combinations are worth investigating further. However, already on the basis of the appearance of the histograms, our preferred choice is "+ − ++" since the large narrow peak on the low-density side indicates the expected uniform density of the aliphatic phase. Next we investigate the electron density profiles of the unit cell for the two phase combinations, "++ − −" and "+ − ++".

Columnar Model. The electron density profiles of the unit cell for the phase combination "++ − −" are shown in Figure 6a at elevations $z = 0$, $z = {}^1/_4$, and $z = {}^1/_2$. Electron density shows continuous ridges, corresponding to linear high-density regions or *columns*, in the zero and half level sections. A third set of columns, this time vertical, can be traced through all three sections in Figure 6a at positions $x = {}^1/_2$, $y = 0$ (with x-axis on the right and y-axis on the left). Thus, according to this model, the structure essentially consists of three mutually perpendicular sets of parallel columns which represent the high electron density regions (aromatic parts) of the molecules. The high-density regions are shown schematically in the model representation of the unit cell in Figure 6b. The three sections at levels $z = 0$, ${}^1/_4$, and ${}^1/_2$ are indicated for easy comparison with Figure 6a. An isolated column is shown separately at the bottom of Figure

(34) Although the intensity of (*hk*0) and (*kh*0) (in general, (*hkl*) and (*khl*)) reflections are equal for the Laue group of the space group *Pm*3*n* the point group symmetry of the space group requires these reflections to have the same or opposite phase depending on whether the sum is even or odd, respectively. Hence the reflections (210) and (120) are treated separately with opposite phases but the same intensity. Accordingly the higher order reflections, (321) and (231), that occur in the electron density computations for the 12G2-AG are treated separately with the same phase and intensity. It appears that in the studies of lyotropic systems this distinction has not been made (Luzzati, V.; Vargas, R.; Mariani, P. *J. Mol. Biol.* **1993**, *229*, 540).

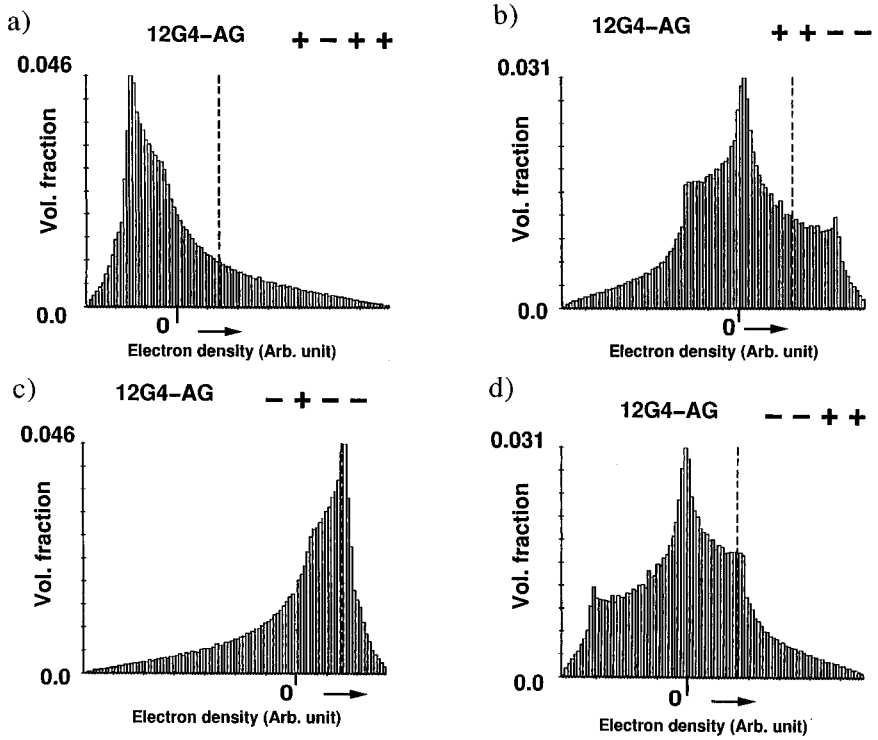

Figure 5. Histograms of electron density distribution for **12G4-AG**. Calculation was based on the intensities of reflections (200), (210), (120), and (211) with the respective phase combinations: (a) + − ++, (b) ++ − −, (c) − + − −, and (d) − − ++.

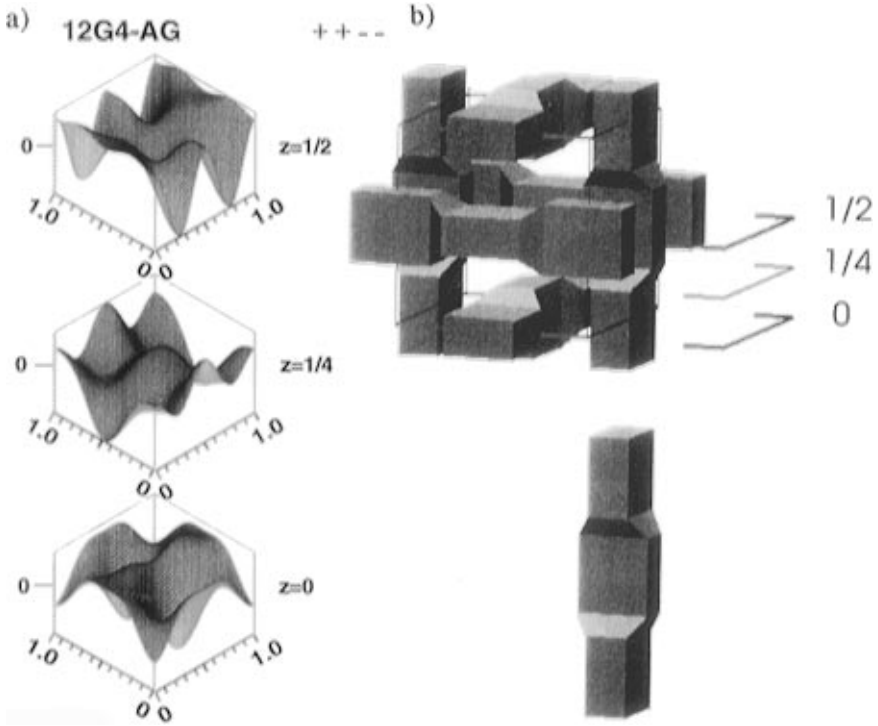

Figure 6. (a) Electron density profiles for **12G4-AG** corresponding to the "columnar" model. They are shown at three elevations: $z = 0$, $^1/_4$, and $^1/_2$. In this and subsequent electron density diagrams the *x*-axis is on the right and the *y*-axis is on the left hand side. (b) Schematic drawing of the columnar model of the cubic structure. The shaded volumes are the high electron density zones. The edges of the unit cell are shown. An isolated column is shown below.

6b. It consists of segments which are flattened alternatively in one of the two mutually perpendicular transverse directions. The electron density along the spine of the column is nearly constant. We refer to the above molecular organization as the columnar cubic model.

If this model was the correct one, the aromatic portions of the **12G4-AG** monodendrons would form infinite continuous columns, surrounded by an aliphatic matrix. However, this is difficult to visualize considering the architecture of **12G4-AG** monodendrons. Furthermore, as there are 16 **12G4-AG** monodendrons and 6 column segments per unit cell, each segment would contain $2^2/_3$, *i.e.*, a noninteger number, of **12G4-AG** monodendrons. These two points suggest that **12G4-AG** is unlikely to form the columnar cubic structure. In fact overwhelming evidence supports the alternative model, as outlined below.

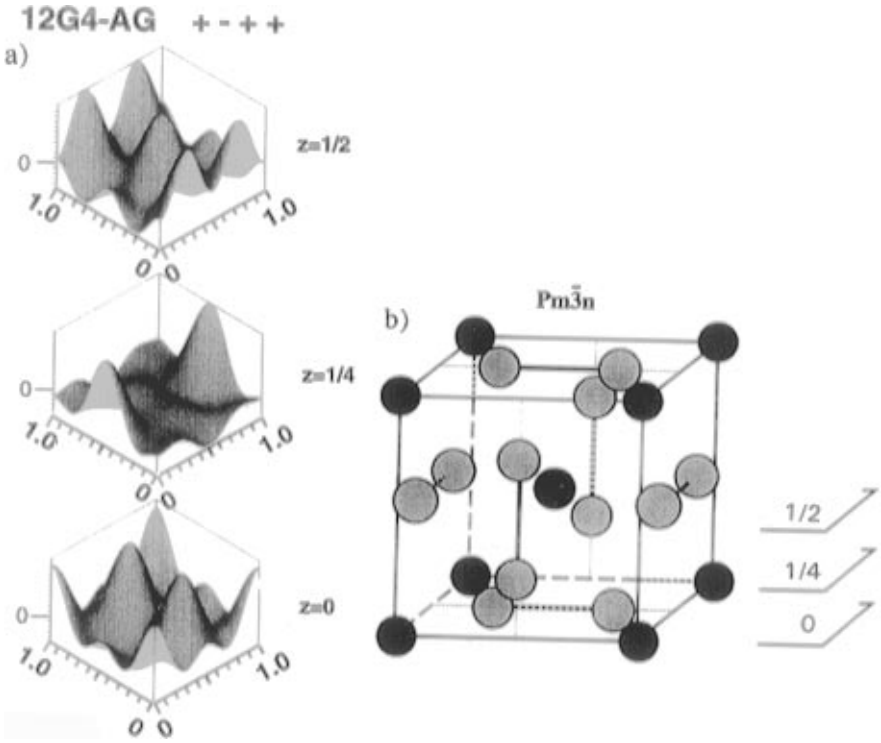

Figure 7. (a) Electron density profiles for the micellar model of **12G4-AG** at $z = 0$, $^1/_4$, and $^1/_2$. (b) Schematic drawing of the unit cell in the micellar model showing the positions of the high electron density regions as spheres. Black spheres at the corners and at the body center of the cubic unit cell are centered on special positions ***a***. Grey spheres at $^1/_4$ and $^3/_4$ positions along face bisectors are centered on special positions ***c***.

Spherical Micellelike Model. The computed electron density profile for the second phase choice, "+ − ++" (Figure 7a), shows large maxima (aromatic regions) at the corners and the body-center (special position ***a***[35]) of the unit cell. In addition, it has large very similar maxima along one of the bisectors of each face at the positions $^1/_4$ and $^3/_4$ (special position ***c***). The three-dimensional contours of the electron density maxima are to a first approximation spherical (see further below for details). The high electron density regions are shown as spheres in the model representation of this structure in Figure 7b. The two types of spheres, on special positions ***a*** and ***c***, are shown as black and grey, respectively. Thus, according to this second model, the aromatic moieties cluster around these special positions forming discrete *micelles* of nearly spherical average shape embedded in aliphatic continuum (micellar model). There are two micelles at positions ***a*** (black) and six at positions ***c*** (grey) per unit cell. There are two **12G4-AG** molecules per micelle (Table 3).

The narrow low-density peak in the histogram (Figure 5b) for this second phase choice is consistent with the intermicellar volume, occupied by aliphatic chains, having nearly constant density. This is illustrated by the large almost flat area between the peaks in the $z = ^1/_4$ profile in Figure 7a. The reason for the absence of the expected distinct high-density peak in the histogram is also apparent from the appearance of the profiles: compared with the majority (80%) aliphatic phase, the minority (20%) aromatic phase is far more affected by the smearing associated with positional disorder (see above). Therefore the small high-density plateau regions expected in Figure 7a at the centers of the micelles are rounded off, and only a broad shoulder rather than a discrete peak is observed in the histogram (Figure 5b).

The spherical micellar model is our preferred choice on grounds of the appearance of the histogram and the electron density profiles as well as on grounds of the integer number of **12G4-AG** monodendrons per structural unit (spherical micelle). Further structural details derived from the richer diffraction pattern from compounds **12G2-AG** and **12G3-AG** corroborate the validity of this model, as described in the next section.

In the micellar model, "+ − ++", the special positions where the electron density has large maxima, *i.e.*, corners, body-center, and $^1/_4$ and $^3/_4$ positions along one of the bisectors of each face, coincide with the positions of biological lipid micelles (spherocylinders) for the type-I (lipid-in-water) lyotropic cubic phase with the same symmetry $Pm\bar{3}n$.[17,34−37] It has been proposed[36,37] that the elongated micelles located at the corners and the body center of the unit cell (special position ***a***) are dynamically disordered giving rise to a spherical electron density distribution. However, such motion would appear unlikely in a closely-packed thermotropic system.

Detailed Structure of the Spherical Supramolecular Dendrimers Self-Assembled from 12G2-AG and 12G3-AG Monodendrons in their Cubic LC Phase. Having opted for the spherical micellar model on the basis of the strong reflections of **12G4-AG**, we proceed by analyzing the diffraction data for **12G2-AG** and **12G3-AG** which contain a larger number of reflections (Table 2). The diffractograms and the corresponding electron density maps of the latter two compounds are very similar and thus the common structure will be discussed here on the example of **12G2-AG**. Altogether six reflections, *i.e.*, all those with significant intensities, were included in the calculation of electron density profiles. In addition to the strong reflections (200), (210), and (211), these now include (220), (321), and (400). As before, the three new reflections provide eight independent choices (but see endnote and ref 34, this time with reference to reflection (321)). All eight possible phase

(35) *International Tables for Crystallography* Hahn, Th., Ed.; Kynoch Press: 1983.

(36) Fontell, K.; Fox, K.; Hansson, E. *Mol. Cryst. Liq. Cryst.* **1985**, *1*, 9.

(37) (a) Eriksson, P.-O.; Lindblom, G.; and Arvidson, G. *J. Phys. Chem.* **1985**, *89*, 1050. (b) Eriksson, P.-O.; Lindblom, G.; and Arvidson, G. *J. Phys. Chem.* **1987**, *91*, 846.

combinations for these additional reflections were investigated. One combination, "+ − − −", stands out in that it does not distort the electron density map relative to that for **12G4-AG** but instead sharpens its features (here the signs refer, respectively, to reflections (220), (321), (231), and (400)). Electron density profiles for the $z = 0$, $z = {}^1/_4$, and $z = {}^1/_2$ sections of the unit cell for the overall phase combination "+ − ++ + − − −" are shown in Figure 5 of Supporting Information. The sharper features of these profiles, which are otherwise rather similar to those in Figure 7a, can be best seen in the $z = {}^1/_4$ section.

At this stage it is appropriate to focus on the fine details of the electron density maps. Thus for example, although the electron density in the intermicellar region at the $z = {}^1/_4$ level appears reasonably flat, closer examination of the contour map (see Figure 8a) reveals relatively small but significant deviations of ρ from the constant value. This contour map should be compared with the model in Figure 8b which shows the $z = {}^1/_4$ plane in relation to the neighboring micelles. The black solid circles in Figure 8a coincide with those in Figure 8b, where they mark the intersections of the $z = {}^1/_4$ plane with the lines connecting the closest pairs of micelles across this plane. Attention is drawn to the fact that all small maxima or shoulders (red contours) in Figure 8a coincide with such intersections. They are thus the result of genuine overlap between spherical micelles and not random distortions of the map. Similarly, the presence of minima in ρ, such as the comparatively deep minimum at $({}^1/_2, 0, {}^1/_4)$, can be traced to the absence of vicinal spherical micelles. Such fine details of the electron density distribution are very sensitive to the phase choice for weak reflections and the internal consistency of the electron density map at all levels is a strong indication that the chosen phase combination is correct.

Finer detail of micellar shape can be observed by comparing the $z = 0$ level contour map in Figure 9 with the $z = {}^1/_4$ level map in Figure 8a. The two crystallographically distinguishable micellar types indeed have somewhat different shapes. The micelles, *i.e.*, the high-density regions, situated at the corners and at the body center of the unit cell (special position ***a***) are spherical to a good approximation. This is evident from the circular contours (corners, Figure 9) and the high site symmetry $m\bar{3}$. On the other hand, micelles at the special positions ***c*** lying on face bisectors have the shape which is best described as rounded tetrahedron. $\bar{4}m.2$ is their site symmetry. In Figure 9 the cross-sections through these latter micelles have the shape of rounded triangles where the apex on the left (right) hand side of the triangle represents the tetrahedron edge normal to the figure plane, while the triangle base on the right (left) represents the tetrahedron edge lying in the figure plane. In Figure 8a the tetrahedra are rotated by 90° around the [010] axis, and, accordingly, their central cross-section now has a form of a rounded square. The tetrahedral micelles are lined up as antiparallel pairs (ABAB stacking) along the three orthogonal face-bisector directions.

The reason for tetrahedral distortion of these micelles is most likely in their tetrahedral coordination. Thus *e.g.* the micelle at $({}^1/_2, {}^1/_4, 0)$ (Figure 9) is surrounded by four micelles at (0, 0, 0), (1, 0, 0), $({}^1/_2, {}^1/_2, {}^1/_2)$, and $({}^1/_2, {}^1/_2, {}^1/_2)$. While tetrahedrally distorted, the micelles lying on face bisectors can, to a first approximation, still be regarded as spherical.

Figure 9 shows a sizeable maximum in electron density in the $z = 0$ plane at the $(0, {}^1/_2, 0)$ position. This does not correspond to a micellar site, but there are two micelles directly above and below this site, each a distance of only 0.25a away; hence the high maximum in the $z = 0$ plane.

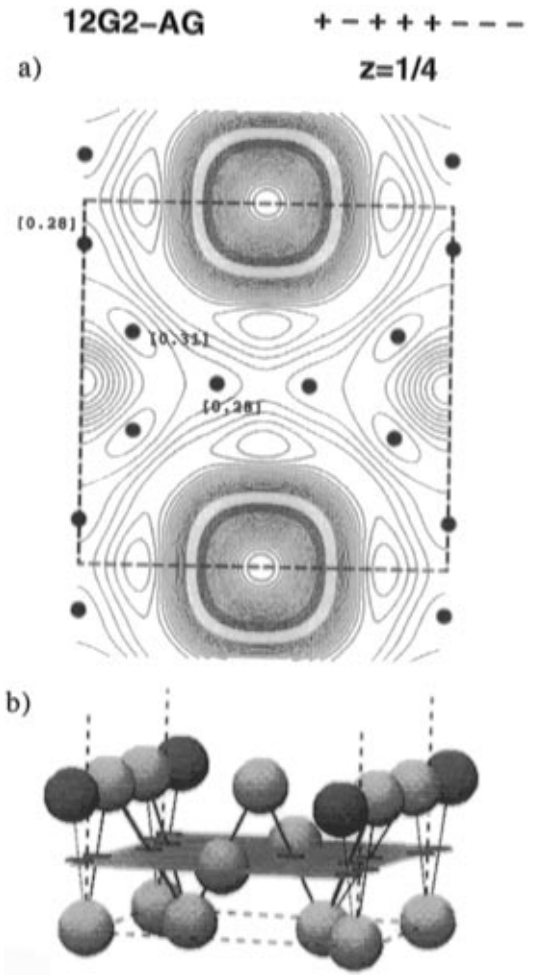

Figure 8. (a) Electron density contour map of the $z = {}^1/_4$ section of the **12G2-AG** unit cell for the phase combination "+ − +++ − − −" (vertical: *x*-axis, horizontal: *y*-axis). The solid circles mark the intersections with the lines joining the nearest micelles at $z = 0$ and $z = {}^1/_2$ levels (compare with Figure 10b). The distances between the micelle centers and the intersection points are shown as fractions of the cell parameter. Black contours represent negative, and red and other colors positive relative electron densities. The thick dashed line delimits the unit cell. (b) Sketch of the lower section of a unit cell showing the $z = {}^1/_4$ plane and the micelles above and below it. The edges of the unit cell are marked by dashed lines. Darker spheres represent micelles outside the unit cell. Lines connecting the nearest neighbour micelles across the $z = {}^1/_4$ plane are shown (full lines).

It may be reiterated that the notion of micelles and their spherical shape refers in these thermotropic systems specifically to the high-density regions, in this case mainly aromatic. When aliphatic regions are included the structure should be regarded in terms of space filling polyhedra. Those polyhedra centered on positions ***a*** (spherical micelles, black circles in Figure 7b) correspond to distorted dodecahedra (12-hedra) and those centered on positions ***c*** (tetrahedrally distorted micelles, grey in Figure 7b) correspond to tetrakaidecahedra (14-hedra).[38]

With more Fourier terms in the electron density summation (eq 3), the sharper features of the maps for **12G2-AG** mean that the plateau in r at the center of a micelle is flatter than in the case of **12G4-AG**. This results in the histogram of **12G2-AG** (see Figure 6 of Supporting Information) having a sharper high-density cutoff compared to that in the **12G4-AG** histogram (Figure 5b). The emergence of a clear high-density shoulder, if not a discrete maximum, is indeed evident in Figure 6 of Supporting Information.

(38) Charvolin, J.; Sadoc, J. F. *J. Phys. France* **1988** *49*, 521.

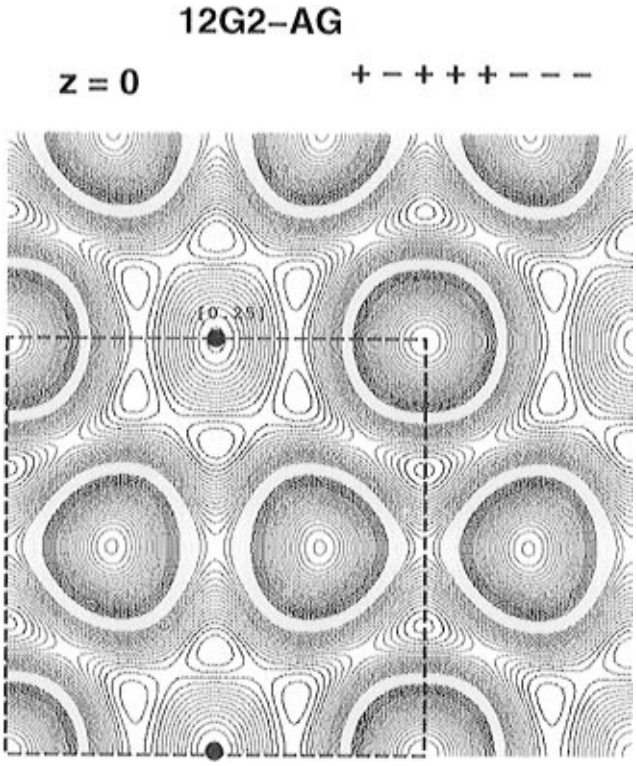

Figure 9. Electron density contour map of the $z = 0$ section of the **12G2-AG** unit cell for the phase combination "+ − +++ − − −" (vertical: *x*-axis, horizontal: *y*-axis). The solid circles mark the intersections with the lines joining the nearest micelles at $z = {}^1/_4$ (compare with Figure 10b). The distances between the micelle centers and the intersection points are shown. Black contours represent negative, and red and other colors positive relative electron densities. The thick dashed line delimits the unit cell.

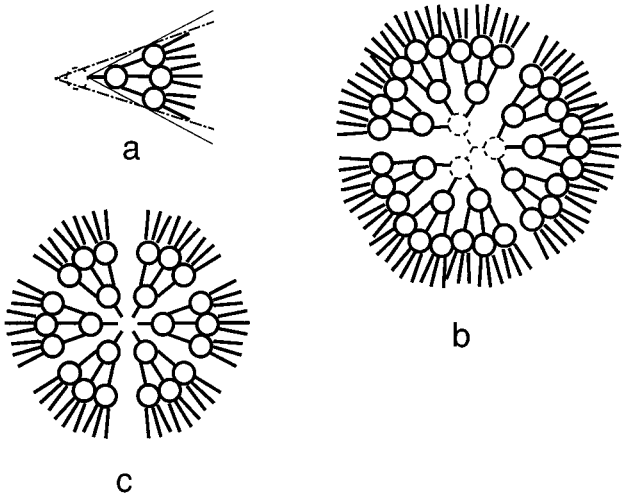

Figure 10. Schematic two-dimensional representation of (a) a **12G2-AG** molecule (full lines) with an added gallic acid group (dashed) illustrating the decreased taper angle per G2 unit in **12G2-AG** relative to that in **12G2-AG**; (b) a hypothetical two-dimensional micelle with nine molecules of **12G2-AG** or three molecules of **12G3-AG**; and (c) a micelle with six molecules of **12G2-AG**.

From the measured macroscopic density and unit cell size the numbers of monodendrons per cell and per supramolecular spherical dendrimer or micelle have been calculated as shown in Table 3. The first set of values in the table (outside brackets) refer to the density of 0.99 g cm^{-3} measured for **12G2-AG**. Assuming that volume contributions from the aromatic and the aliphatic regions of the molecule are additive, it can be easily shown that the density variation between **12G2-AG**, **12G3-AG**, and **12G4-AG** are well within 0.01 g cm^{-3}. The density of 0.99 g cm^{-3} is considered as the lower bound since densification was found to be a slow process requiring prolonged annealing. Assuming that monodendrons are equally distributed among all supramolecular spherical dendrimers or micelles there are, respectively, 11.3, 5.8, and 1.9 monodendrons per supramolecular micellar dendrimer in **12G2-AG**, **12G3-AG**, and **12G4-AG**. The latter value strongly suggests that there are in fact two molecules per micelle in **12G4-AG**, a number which is obtained exactly with a density of 1.04 g cm^{-3}. In fact, if this density is assumed for all compounds studied, integer numbers of monodendrons per supramolecular spherical dendrimer or micelle are obtained in all cases (values in brackets in Table 3).

Similarities between Thermotropic and Lyotropic Systems. This study has confirmed the validity of the hypothesis put forward in the Introduction by demonstrating that systematic variation in the molecular architecture of the monodendron can change the shape of the supermolecule generated by their self-assembly from column to spherical and of the resulted phase from columnar hexagonal to cubic. The primary factor effecting this change is the transition from flat tapered to conical monodendron. Thus while compounds of the flat tapered shape type (Scheme 1) (**12ABG**) invariably form the hexagonal columnar LC phase,[10] the equivalent compound **12G2-AG**, being more conical, shows the LC micellar cubic phase. By analogy with inverse lyotropic LC phases, the conical monodendron can be expressed as the mean curvature c_m of the aromatic-aliphatic interface being increasingly negative. While discussing the analogy with lyotropic phases, we notice in passing that the $Pm\bar{3}n$ cubic phase has never been observed in inverse (Type II) lyotropics. So far the only observed Type II cubic phase, *i.e.*, one in which aliphatic chains form the continuous matrix, is of $Fd\bar{3}m$ symmetry.[18b]

Correlation between Monodendron Generation and Size of Supramolecular Spherical Dendrimer. To the extent that the molecular building blocks forming columnar structures can be described as flat tapered or fan-like **12-ABG** (*i.e.*, **4-m-12G2AG**, *i.e.*, Scheme 1a),[10] in the present cubic phase the building blocks responsible for the generation of spherical micelles may be regarded as conical **12G2-AG** (*i.e.*, **3,4,5-t-12G2-AG**) and **12G3-AG** (*i.e.*, **3,4,5-t-12G3-AG**) and as hemispherical in the case of **12G4-AG** (*i.e.*, **3,4,5-t-12G4-AG**).

It is interesting to compare the numbers of monodendrons per supramolecular spherical micellar aggregate for the three generations studied. Comparing first the supramolecular assemblies generated from **12G4-AG** and **12G3-AG**, there are two monodendrons in a spherical micelle in the former case and six monodendrons in the latter case (Table 3). The observed ratio of three between these two cases is expected since this is close to the ratio of molecular masses and volumes (volume ratio 3.01). However, the spherical micelles generated from **12G2-AG** contain only 12 rather than the expected 18 monodendrons, *i.e.*, only twice rather than three times the number found in the micelles of **12G3-AG**. This is in spite of the fact that the volume ratio between **12G3-AG** and **12G2-AG** molecules is again close to three (precisely 3.03). Consequently there is a reduction of about one-third in the volume of a micelle and therefore of the whole unit cell on going from **12G3-AG** to **12G2-AG** (see Table 3). We suggest that the smaller than expected supramolecular micelles obtained from **12G2-AG** are due to the somewhat larger molecular taper in this lower generation monodendron. The argument is illustrated on hypothetical two-dimensional examples in Figure 10. Figure 10a shows schematically a **12G2-AG** molecule (solid lines)

which we may assume to have a taper angle close to $2\pi/6$ radians (thin solid lines); the additional gallic acid present in the molecule of **12G3-AG** is also shown (dashed lines) to illustrate the reduced taper of each of its three G2 constituents. Assuming, by way of example, that the conical building block is reduced from $\sim 2\pi/6$ to $\sim 2\pi/9$ radians (dash-dot lines), we may expect optimal packing in a two-dimensional spherical micelle to be achieved either with six molecules of **12G2-AG** (Figure 10c) or with nine-thirds, *i.e.*, three molecules, of **12G3-AG** (Figure 10b). Figure 10b also illustrates a large vacancy which would form in the center of a spherical supramolecular micelle of **12G2-AG** should it have been made up of nine instead of six molecules (solid lines).

Reverting to the real three-dimensional cases, six appears to be the optimal number of monodendrons for packing into a spherical supramolecular dendrimer or micelle in the case of **12G3-AG**, and, therefore, we associate with these molecule a taper described by a solid angle close to $4\pi/6$ steradians. The taper of molecules of **12G2-AG** is, however, larger than one-third of the above value, apparently being close to $4\pi/12$ rather than to $4\pi/18$. Moving in the direction of higher monodendron generations, the number of **12G4-AG** molecules in a spherical micelle is only one third that in the case of **12G3-AG** (Table 3), suggesting that the **12G4-AG** monodendrons are hemispherical with a solid angle of $4\pi/2$. Analogy with the above comparison between **12G2-AG** and **12G3-AG** would in fact suggest a somewhat lower *natural* taper of an isolated **12G4-AG** molecule. However, since the choice in the case of **12G4-AG** is limited to either two or three molecules per micelle, the former is adopted by the monodendron, with the corresponding taper angle of $4\pi/2$. The fact that this value is not coincident with the *natural* taper of **12G4-AG** is suggested by the fact that the cubic phase of the supramolecular dendrimer generated from two **12G4-AG** does not form readily and that its formation requires elaborate and prolonged thermal treatment. Qualitative comparison shows that cubic phase formation rates are equally high in **12G3-AG** and **12G2-AG** and substantially lower in **12G4-AG**. This suggests that the match between the *natural* taper and that adopted in a micelle (integral fraction of 4π) is good for both of the former but rather poor for the latter compound. The substantially lower clearing temperature of the cubic phase of **12G4-AG** relative to that of **12G2-AG** and **12G3-AG** (Table 1) also indicates a lower stability and thus poorer packing in the cubic phase resulted from **12G4-AG**.

The above simplified scheme appears to explain the experimentally obtained variation in the number of molecules and molecular residues per micelle and the variation in unit cell size with changing monodendron generation. In terms of mean curvature c_m of the aromatic−aliphatic interface, this is directly related to the molecular shape. The absolute value $|c_m|$ is larger for a molecule of **12G2-AG** compared to that for **12G3-AG**. Thus it is also larger for a micelle of **12G2-AG** (smaller radius) compared to that for a micelle of **12G3-AG**.

Vacancies. The shapes of the micelles have already been discussed in the section on detailed structure of **12G2-AG** and **12G3-AG**. It was established that the micelles at special positions ***a*** (corners and body center) are spherical, while those on positions ***c*** (on face bisectors) are tetrahedrally distorted spheres. It is also of interest to examine the positions and shapes of the minima in electron density. As already mentioned, there is a conspicuous minimum at ($^1/_2$, 0, $^1/_4$) (Figure 8a). Its shape is that of a rounded tetrahedron. This is due to tetrahedral placement of the four nearest micelles at ($^1/_2$, $^1/_4$, 0), ($^1/_2$, $^1/_4$, 0), ($^1/_4$, 0, $^1/_2$), and ($^3/_4$, 0, $^1/_2$). It will be noted that this tetrahedral vacancy is centered on a special position ***d***. The ***d***-set of special positions is equivalent to the ***c***-set, having the same site symmetry $\bar{4}m.2$. It is not surprising to find electron density minima at ***d*** if one considers the space filling of the micellar $Pm\bar{3}n$ cubic lattice as a hypothetical two-stage process. In the first stage the body-centered lattice is established with the micelles taking up positions ***a***. There remains room for six more micelles with their associated aliphatic sheaths and either of the two sets ***d*** and ***c***, with six special positions each, is equally available. As one of the sets is occupied (***c***) the positions of the alternative set (***d***) remain the loci of low density.

As can be seen in Figure 9, density minima as deep as those at positions ***d*** also exist elsewhere—*cf.* the six minima surrounding the (0, $^1/_2$, 0) position. All these minima are the locations where alkyl chain ends (methyl groups) are expected to be found preferentially (termed *chaotic zones* by Luzzati and co-workers).[17d] The depth of the density minima are considered to play a key role in determining the stability of the mesophase.[39] These vacancies can be found at points where the distance from the center of the nearest micelle is greatest. For example the distance between a position ***d*** and the center of the nearest micelle is 0.354a, *i.e.*, 24 Å in the case of **12G2-AG**. In comparison, the distance between the carboxylic hydrogen and the end of an extended dodecyl chain in **12G2-AG** is 26 Å, *i.e.*, only 2 Å larger. It follows that such a chain must be almost completely extended to reach position ***d*** if the carboxylic end of the molecule is anchored to the micellar center by hydrogen bonding. The free energy of the system must therefore be balanced between an energetic space-filling term and an entropic term which opposes chain extension.[40]

Geometrical comparison between molecular model dimensions and the distance of the vacancy from nearest-neighbor micelles have also been made for supramolecular dendrimers of other generations and the results are shown in Table 3. The excess molecular length over the micelle-vacancy distance is seen to increase with increasing generation number. By analogy the reverse may also be assumed which means that the first generation monodendrons might be too short to form the $Pm\bar{3}n$ phase. This is believed to be the reason for **12G1-AG** not showing the cubic phase (Figure 3 Supporting Information). Equally, it may be expected that molecules equivalent to **12G2-AG** but having shorter chains (e.g., decyloxy instead of dodecyloxy) may also not be able to reach as far as positions ***d*** and thus may not form the present cubic phase. These and other possibilities are currently being investigated.

Driving Force for Self-Assembly. A self-assembly event can be dominated by a single molecular recognition process based on directional and attractive forces such as hydrogen bonding, van der Waals, electrostatic, and hydrophobic interactions. However, these processes are cooperative, and their cooperative contribution could be equally important not only in the aggregation process but also particularly in the stabilization of a particular architecture.[41] Previous experiments from our[10] and other laboratories[6] have demonstrated the use of hydrogen bonding, electrostatic and van der Waals interactions to dominate the self-assembly of supramolecular dendrimers from functional monodendrons. An inspection of the results from Table 1 reveals that the thermodynamic stability of the cubic LC phase generated from identical generations of mono-

(39) Seddon, J. M. *Biochim. Biophys. Acta* **1990**, *1031*, 1.

(40) Kirk, G. L.; Gruner, S. M.; Stein, D. L. *Biochemistry* **1984**, *23*, 1093.

(41) (a) Delaage, M. in *Molecular Recognition Mechanisms*; Delaage, M., Ed.; VCH: Weinheim, 1991; p 1. (b) Buckingham A. D. In *Principles of Molecular Recognition*; Buckingham, A. D.; Legon, A. C.; Roberts, S. M. Eds.; Chapman and Hall: New York, 1993, p 1. (c) Schneider, H.-J. *Angew. Chem., Int. Ed. Engl.* **1991**, *30*, 1417. (d) Tanford, C. *Science* **1978**, *200*, 1012.

dendrons decreases in the following order: **12Gn-AG** > **12Gn-AG-CH_2OH** > **12Gn-AG-CH_3**. This stability is indicated by the corresponding isotropization temperature. The cubic LC phases generated from these monodendrons are isomorphic, and more details on this issue will be published elsewhere. Therefore, the stability of the cubic LC phase is determined by the stability of the spherical supramolecular dendrimer. This indicates, as in previous systems,[10] that H-bonding from −COOH, followed by H-bonding from $-CH_2OH$ groups, in that order favors the aggegation of a monodendron in a supramolecular dendrimer. In addition, monodendrons **12Gn-AG-CH_3** which do not have a H-bonding source, self-assemble into spherical dendrimers of lower stability. This demonstates that van der Waals interactions between the CH_2 groups and those between the aromatic groups can be solely responsible for this self-assembly process. Therefore, they must also have an important contribution in the case of the self-assembly of **12Gn-AG-CH_2OH** and **12Gn-AG**. Previously, only van der Waals interactions induced by fluorophobic effect were shown to solely be able to aggregate a supramolecular dendrimer.[10h] More details on these and other systems which self assemble *via* van der Waals interactions and on the assembly mechanism will be published elsewhere.

Conclusions

The cone-shaped monodendrons **12Gn-AG** with $n = 2$, 3 and the hemispherical one with $n = 4$ form a novel thermotropic LC cubic phase with symmetry $Pm\bar{3}n$. Studies of electron density profiles and histograms computed from the X-ray diffraction data demonstrate based on a micellar like model that self-assembled supramolecular dendrimers with the aromatic regions centered around the corners, body-center, and the $^1/_4$ and $^3/_4$ positions along one of the bisectors of each face are formed. This model is quite similar to that accepted for the lyotropic phase with the same symmetry. All supramolecular dendrimers can be well approximated by a spherical shape. However, those which lie on face bisectors are in fact highly rounded tetrahedra. The averaged shape of a monodendron is conical or wedge-like in the case of **12G2-AG** and **12G3-AG** and hemispherical in **12G4-AG**. The solid angle subtended at the micellar center by a peripheral alkoxy chain cross-section decreases with increasing monodendron generation. This leads to an increase in the size of micelles and of the entire unit cell as one moves from **12G2-AG** to **12G4-AG**.

Comparatively fine structural detail obtained helps elucidate certain features regulating the stability of the cubic mesophase. For example, from the position and depth of density minima it is predicted and experimentally demonstrated that the $Pm\bar{3}n$ phase does not form in the first generation monodendron **12G1-AG** and may not form in the second generation monodendrons containing shorter alkyl chains. Further isomorphous replacement studies of this type of monodendron molecules having partially fluorinated alkyl regions and of their salts with heavy metals are under way. The present is the first example of the rational design of monodendrons which self-assemble into supramolecular spherical dendrimers and the first quantitative structural characterization of their shape, size, and structure with the aid of a novel thermotropic cubic LC phase. These conclusive structural experiments were possible, because the liquid-like short-range interactions of the cubic phase provided the long-range periodicity necessary for detailed electron mapping by X-ray diffraction. The use of this novel shape of thermotropic soft order[42] in the design of new macromolecular and supramolecular systems[43] with more complex architectures and their potential technological applications will be addressed in future publications.

Experimental Section

Materials. $LiAlH_4$ (95+%), $SOCl_2$ (99+%), 2,6-di-*tert*-butylpyridine (97%), methyl 3,4,5-trihydroxybenzoate (98%), and anhydrous K_2CO_3 (all from Aldrich) were used as received. NMP, DMF and CH_2Cl_2 (all ACS reagent from Fisher) were dried over CaH_2 and distilled. Et_2O (Fisher) was refluxed over sodium benzophenone ketyl and distilled freshly before use.

General Methods. ^{1}H NMR (200 MHz), ^{19}F NMR (188 MHz), and ^{13}C NMR (50 MHz) spectra were recorded on a Varian Gemini 200 spectrometer. The purity of products was determined by a combination of TLC on silica gel plates (Kodak) with fluorescent indicator, NMR spectroscopy, elemental analysis, matrix assisted laser desorption ionization time-of-flight (MALDI-TOF) mass spectrometry, GPC, and HPLC. MALDI-TOF was performed on a Finnigan Vision 2000 TOF mass spectrometer with 3,5-dihydroxybenzoic acid matrix. A Perkin-Elmer Series 10 HPLC equipped with an LC-100 column oven, Nelson Analytical 900 Series integrator data station, and two Perkin-Elmer PL gel columns of 5×10^2 and 1×10^4 Å was used in both HPLC and GPC mode. THF was used as solvent at the oven temperature of 40 °C unless otherwise noted. Detection was by UV absorbance at 254 nm. Polystyrene standards ($1.02 \leq M_w/M_n \leq 1.13$) were used to construct the calibration curve. Thermal transitions were measured on a Perkin Elmer DSC-7. Zn and In were used as calibration standards. In all cases, the heating and cooling rates were 10 °C min^{-1} unless otherwise noted. First order transition temperatures were reported as the maxima and minima of their endothermic and exothermic peaks. Glass transition temperatures (T_g) were read at the middle of the change in heat capacity. Small-angle diffraction (SAXD) from powder specimens was recorded with a quadrant detector at Station 8.2 of the Synchotron Radiation Source at Daresbury, UK. Small and wide-angle diffraction from monodomain samples was recorded with an image plate area detector (MarResearch) using graphite-monochromatized CuKα radiation. In both cases samples in capillaries were held in a custom-built temperature cell controlled to within ±0.1 °C. The beampath up to the beamstop was either evacuated or flushed with N_2.

Synthesis. The synthesis and characterization of methyl 3,4,5-tris(*n*-dodecan-1-yloxy)benzoate (**12G1-AG-CH_3**) and 3,4,5-tris(*n*-dodecan-1-yloxy)benzoic acid (**12G1-AG**) were described previously.[10a,d]

General Procedure for the Synthesis of 12Gn-AG-CH_2OH. Synthesis of 3,4,5-Tris(*n*-dodecan-1-yloxy)benzyl Alcohol (12G1-AG-CH_2OH). **12G1-AG-CH_2OH** was obtained by the reduction of **12G1-AG** with $LiAlH_4$. To a suspension of 2.17 g (55.5 mmol) of $LiAlH_4$ in 50 mL of anhydrous Et_2O **12G1-AG-CH_3** was added dropwise and the mixture was stirred for 1 h at room temperature under N_2 after which time TLC and ^{1}H NMR analyses (δ 7.25, δ 3.89 disappeared) indicated complete conversion. The reaction was quenched by dropwise, addition of 2 mL of H_2O, 2 mL of 15% NaOH, and 6 mL of H_2O. The granular salts were filtered and rinsed with THF. Evaporation of the solvent afforded a white solid which upon recrystallization from acetone at 4 °C yielded 45.7 g (93.4%) of a white powder. Thermal transitions are recorded in Table 1. Purity (HPLC), 99+%; TLC (hexanes:ethyl acetate, 5:1): $R_f = 0.21$. ^{1}H NMR ($CDCl_3$, TMS, δ, ppm): 0.88 (t, 9H, $CH_3(CH_2)_{11}$, $J = 6.1$ Hz), 1.26 (overlapped peaks, 48H, $CH_3(CH_2)_8$), 1.45 (m, 6H, $CH_3(CH_2)_8CH_2$), 1.80 (m, 6H, CH_2CH_2OAr), 3.94 (t, 2H, CH_2OAr, 4 position, $J = 6.8$ Hz), 3.97 (t, 4H, CH_2OAr, 3,5 positions, $J = 7.0$ Hz), 4.59 (d, 2H, CH_2OH), 6.56 (s, 2H, *ortho* to CH_2OH); ^{13}C NMR ($CDCl_3$, δ, ppm): 14.0 (CH_3), 22.6 (CH_3CH_2), 26.1 ($CH_2CH_2CH_2OAr$), 29.4 ($CH_3(CH_2)_2CH_2$), 29.6 ($CH_3(CH_2)_3(CH_2)_5$), 30.3 (CH_2CH_2OAr), 31.9 ($CH_3CH_2CH_2$), 65.4 (CH_2OH), 69.0 (CH_2OAr, 3,5 positions), 73.4 (CH_2OAr, 4 position), 105.1 (*ortho* to CH_2OH), 136.2 (*para* to CH_2OH), 137.5 (*ipso* to CH_2), 153.1 (*meta* to CH_2OH).

Synthesis of 3,4,5-Tris(*n*-dodecan-1-yloxy)benzyl Chloride (12G1-AG-CH_2Cl). **12G1-AG-CH_2Cl** was prepared by chlorination of **12G1-**

(42) deGennes, P.-G. *Angew. Chem., Int. Ed. Engl.* **1992**, *31*, 842.
(43) Lehn, J. M. *Supramolecular Chemistry*, VCH: Weinheim, 1995.
(44) Nystrom, R. F.; Brown, W. G. *J. Am. Chem. Soc.* **1947**, *69*, 1197.

AG-CH_2OH with $SOCl_2$. To a solution of 45.7 g (69.1 mmol) of **12G1-AG-CH_2OH** in 460 mL of dry CH_2Cl_2, a catalytic amount (1 mL) of DMF, followed by 11.5 g (96.8 mmol) of $SOCl_2$ (dropwise) was added with stirring. Approximately 30 min after the addition of $SOCl_2$ the reaction was complete (TLC, $R_f = 0.5$; 20:1 hexanes:ethyl acetate). The solvent and excess $SOCl_2$ were distilled under vacuum. The resulting white solid was dissolved in Et_2O, washed three times with H_2O, dried over $MgSO_4$, and filtered, and the solvent was rotoevaporated. After vacuum drying for 1 h, 42.8 g (91.1%) of white powder was obtained, mp 47−47.5 °C. Purity (HPLC), 99+%. ^{1}H NMR ($CDCl_3$, TMS, δ, ppm): 0.89 (t, 9H, CH_3(CH_2)$_{11}$, $J = 6.2$ Hz), 1.28 (overlapped peaks, 48H, CH$_3$(CH_2)$_8$), 1.47 (m, 6H, CH$_3$(CH$_2$)$_8$CH_2), 1.77 (m, 6H, CH_2CH$_2$OAr), 3.95 (t, 2H, CH_2OAr, 4 position, $J = 6.5$ Hz), 3.98 (t, 4H, CH_2OAr, 3,5 positions, $J = 6.4$ Hz), 4.51 (s, 2H, CH_2Cl), 6.58 (s, 2H, *ortho* to CH_2Cl); ^{13}C NMR ($CDCl_3$, δ, ppm): 14.1 (*C*H$_3$), 22.7 (CH$_3$*C*H$_2$), 26.1 (*C*H$_2$CH$_2$CH$_2$OAr), 29.4 (CH$_3$-(CH$_2$)$_2$*C*H$_2$), 29.6 (CH$_3$(CH$_2$)$_3$(*C*H$_2$)$_5$), 30.3 (*C*H$_2$CH$_2$OAr), 31.9 (CH$_3$-CH$_2$*C*H$_2$), 46.9 (*C*H$_2$Cl), 69.1 (*C*H$_2$OAr, 3,5 positions), 73.4 (*C*H$_2$OAr, 4 position), 107.0 (*ortho* to CH_2Cl), 132.3 (*para* to CH_2Cl), 138.3 (*ipso* to CH_2), 153.2 (*meta* to CH_2Cl).

Methyl 3,4,5-Tris[3′,4′,5′-tris(*n*-dodecan-1-yloxy)benzyloxy)]benzoate (12G2-AG-CH_3). **12G2-AG-CH_3** was obtained by the alkylation of methyl 3,4,5-trihydroxybenzoate with **12G1-AG-CH_2Cl**. A mixture of K_2CO_3 (23.1 g, 0.167 mmol) in 280 mL of dry DMF was purged for 1 h with N_2. Methyl 3,4,5-trihydroxybenzoate (3.43 g, 18.6 mmol) was added, and the mixture was heated to 65 °C. A solution of **12G1-AG-CH_2Cl** (38.0 g, 55.9 mmol) in 220 mL of DMF was added rapidly. After 1.5 h, the conversion was 91% (^{1}H NMR analysis). No side products were detected. After 3.5 h, the completed reaction mixture was poured into ice-H_2O. The precipitated product was filtered and recrystallized from a mixture of CH_2Cl_2 and MeOH to obtain a light tan powder. Further purification by column chromatography (b. Al_2O_3; CH_2Cl_2) yielded 34.6 g (88.0%) of a white powder. Purity (GPC), 99+%; TLC (20:1 hexanes:ethyl acetate), $R_f = 0.20$. ^{1}H NMR ($CDCl_3$, δ, ppm, TMS): 0.88 (t, 27H, CH_3(CH$_2$)$_{11}$, $J = 6.4$ Hz), 1.26−1.43 (overlapped peaks, 162H, CH$_3$(CH_2)$_8$), 1.71 (m, 18H, CH_2CH$_2$OAr), 3.75 (t, 4H, CH_2OAr, 4-(3′,5′) position, $J = 6.4$ Hz), 3.88 (t, 8H, 3,5-(3′,5′) positions, $J = 6.4$ Hz), 3.88 (s, 3H, CO_2CH_3), 3.93 (t, 6H, CH$_2$-OAr, 3,4,5-(4′) positions, $J = 6.5$ Hz), 5.03 (s, 6H, ArCH_2OAr), 6.60 (s, 2H, *ortho* to CH_2, 4′ position), 6.63 (s, 4H, *ortho* to CH_2, 3′,5′ position), 7.38 (s, 2H, *ortho* to CO_2CH_3). ^{13}C NMR ($CDCl_3$, δ, ppm, TMS): 14.1 (*C*H$_3$), 22.7 (CH$_3$*C*H$_2$), 26.2 (*C*H$_2$CH$_2$CH$_2$OAr), 29.4 (CH$_3$-(CH$_2$)$_2$*C*H$_2$), 29.7 (CH$_3$(CH$_2$)$_3$(*C*H$_2$)$_5$), 30.4 (*C*H$_2$CH$_2$OAr), 31.9 (CH$_3$-CH$_2$*C*H$_2$), 52.2 (CO_2*C*H$_3$), 69.1 (CH$_2$*C*H$_2$OAr, 3,4,5-(3′,5′) positions), 71.7 (Ar*C*H$_2$OAr, 3,5 positions), 73.4 (CH$_2$*C*H$_2$OAr, 3,4,5-(4′) positions), 75.1 (Ar*C*H$_2$OAr, 4 position), 105.7 (*ortho* to CH_2, 3,5 positions), 106.2 (*ortho* to CH_2, 4 position), 109.6 (*ortho* to CO_2CH_3), 125.1 (*ipso* to CO_2CH_3), 131.7 (*para* to CH_2, 3,5 position), 132.4 (*para* to CH_2, 4 position), 137.8 (*ipso* to CH_2, 3,4,5 position), 142.1 (*para* to CO_2CH_3), 152.5 (*meta* to CO_2CH_3), 153.0 (*meta* to CH_2, 4 position), 153.3 (*meta* to CH_2, 3,5 position), 166.5 (*C*O$_2$CH$_3$). Anal Calcd for $C_{137}H_{242}O_{14}$: C, 77.86; H, 11.54. Found: C, 77.93; H, 11.64.

3,4,5-Tris[3′,4′,5′-tris(*n*-dodecan-1-yloxy)benzyloxy)]benzyl Alcohol (12G2-AG-CH_2OH). From **12G2-AG-CH_3** (8.00 g, 3.79 mmol) and $LiAlH_4$ (0.15 g, 35 mmol) were obtained 7.3 g (91.%) of a white solid (after recrystallization from acetone). Purity (GPC), 99+%; TLC (CH_2Cl_2): $R_f = 0.3$. ^{1}H NMR ($CDCl_3$, δ, ppm, TMS): 0.88 (t, 27H, CH_3(CH$_2$)$_{11}$, $J = 6.4$ Hz), 1.26−1.43 (overlapped peaks, 162H, CH$_3$(CH_2)$_8$), 1.70 (m, 18H, CH_2CH$_2$OAr), 3.77 (t, 4H, CH_2OAr, 4-(3′,5′) position, $J = 6.4$ Hz), 3.88 (t, 8H, 3,5-(3′,5′) positions, $J = 6.4$ Hz), 3.92 (t, 6H, CH$_2$OAr, 3,4,5-(4′) positions, $J = 6.5$ Hz), 4.56 (d, 2H, CH_2OH, $J = 6.02$ Hz), 4.97 (s, 2H, ArCH_2OAr, 4 position), 5.01 (s, 4H, ArCH_2OAr, 3,5 positions), 6.62 (s, 4H, *ortho* to CH_2, 3,5 positions), 6.63 (s, 2H, *ortho* to CH_2OH), 6.67 (s, 2H, *ortho* to CH_2, 4 position). ^{13}C NMR ($CDCl_3$, δ, ppm, TMS): 14.1 (*C*H$_3$), 22.7 (CH$_3$*C*H$_2$), 26.2 (*C*H$_2$CH$_2$CH$_2$OAr), 29.4 (CH$_3$(CH$_2$)$_2$*C*H$_2$), 29.5, 29.7 (CH$_3$(CH$_2$)$_3$(*C*H$_2$)$_5$), 30.4 (*C*H$_2$CH$_2$OAr), 31.9 (CH$_3$CH$_2$*C*H$_2$), 65.2 (CH_2OH), 69.0 (CH$_2$*C*H$_2$-OAr, 3,4,5-(3′,5′) positions), 71.5 (Ar*C*H$_2$OAr, 3,5 positions), 73.3 (CH$_2$*C*H$_2$OAr, 3,4,5-(4′) positions), 75.2 (Ar*C*H$_2$OAr, 4 position), 105.5 (*ortho* to CH_2, 3,5 position), 106.2 (*ortho* to CH_2, 4 position), 106.8 (*ortho* to CH_2OH), 132.1 (*para* to CH_2, 3,5 positions), 132.8 (*para* to CH_2, 4 position, *para* to CH_2OH), 136.7 (*ipso* to CH_2OH), 137.6 (*ipso* to CH_2, 3,4,5 positions), 153.0 (*meta* to CH_2, 4 position, *meta* to CH_2-OH), 153.2 (*meta* to CH_2, 3,5 positions). Anal Calcd for $C_{136}H_{242}O_{13}$: C, 78.33; H, 11.70. Found: C, 78.16; H, 11.66.

General Procedure for the Synthesis of 12Gn-AG-CH_2Cl (n > 1). 3,4,5-Tris[3′,4′,5′-tris(*n*-dodecan-1-yloxy)benzyloxy)]benzyl Chloride (12G2-AG-CH_2Cl). **12G2-AG-CH_2OH** (6.0 g, 2.9 mmol) was dissolved in 60 mL of dry CH_2Cl_2. 2,6-Di-*tert*-butylpyridine (1.5 g, 8.1 mmol), DMF (several drops), and $SOCl_2$ (0.48 g, 4.1 mmol) were added dropwise. After complete addition, the reaction was monitored by ^{1}H NMR. Within few minutes, a complete conversion was observed. The product was freeze-dried from benzene solution to obtain a white powder which was used immediately in the next step without further purification. A sample free of 2,6-di-*tert*-butylpyridine was obtained for analytical purposes by precipitation from CH_2Cl_2 into acetone. TLC (20:1 hexanes:ethyl acetate): $R_f = 0.5$. ^{1}H NMR ($CDCl_3$, δ, ppm, TMS): 0.88 (t, 27H, CH_3(CH$_2$)$_{11}$, $J = 6.0$ Hz), 1.26−1.41 (overlapped peaks, 162H, CH$_3$(CH_2)$_8$), 1.74 (m, 18H, CH_2CH$_2$OAr), 3.76 (t, 4H, CH_2OAr, 4-(3′,5′) position, $J = 5.9$ Hz), 3.88 (t, 8H, 3,5-(3′,5′) positions, $J = 6.3$ Hz), 3.91 (t, 6H, CH$_2$OAr, 3,4,5-(4′) positions, $J = 6.3$ Hz), 4.47 (s, 2H, CH_2Cl), 4.96 (s, 2H, ArCH_2OAr, 4 position), 4.99 (s, 4H, ArCH_2OAr, 3,5 positions), 6.60 (s, 4H, *ortho* to CH_2, 3,5 positions), 6.67 (s, 2H, *ortho* to CH_2, 4 position), 7.26 (s, 2H, *ortho* to CH_2Cl). ^{13}C NMR ($CDCl_3$, δ, ppm, TMS): 14.1 (*C*H$_3$), 22.7 (CH$_3$*C*H$_2$), 26.2 (*C*H$_2$CH$_2$CH$_2$OAr), 29.4 (CH$_3$(CH$_2$)$_2$*C*H$_2$), 29.7 (CH$_3$(CH$_2$)$_3$(*C*H$_2$)$_5$), 30.4 (*C*H$_2$CH$_2$OAr), 31.9 (CH$_3$CH$_2$*C*H$_2$), 46.6 (C*H*$_2$Cl), 69.0 (CH$_2$*C*H$_2$-OAr, 3,4,5-(3′,5′) positions), 71.7 (Ar*C*H$_2$OAr, 3,5 positions), 73.3 (CH$_2$*C*H$_2$OAr, 3,4,5-(4′) positions), 75.2 (Ar*C*H$_2$OAr, 4 position), 105.6 (*ortho* to CH_2, 3,5 positions), 106.2 (*ortho* to CH_2, 4 position), 108.8 (*ortho* to CH_2Cl), 131.9 (*para* to CH_2, 3,5 positions), 132.6 (*para* to CH_2, 4 position), 132.9 (*para* to CH_2Cl), 137.8 (*ipso* to CH_2, 3,4,5 positions), 138.6 (*ipso* to CH_2Cl), 153.0 (*meta* to CH_2, 4 position, *meta* to CH_2Cl), 153.2 (*meta* to CH_2, 3,5 positions).

Methyl 3,4,5-Tris{3′,4′,5′-tris[3″,4″,5″-tris(*n*-dodecan-1-yloxybenzyloxy)benzyloxy]benzyloxy}benzoate (12G3-AG-CH_3). A mixture of K_2CO_3 (3.29 g, 23.9 mmol) and 230 mL of dry NMP was purged for 0.5 h with N_2. Methyl 3,4,5-trihydroxybenzoate (0.489 g, 2.65 mmol) was added, and the mixture was heated to 90 °C. A slurry of **12G2-AG-CH_2Cl** (16.7 g, 7.96 mmol) in 100 mL of warm NMP was added rapidly. After 2 h, a 92% conversion was determined by ^{1}H NMR. No side products were detected. After 4 h, the completed hot reaction mixture was poured into 1.5 L of ice−H_2O, and the precipitated solid was filtered. The moist solid was dissolved in Et_2O, washed with H_2O, and dried over $MgSO_4$. Purification by column chromatography (b. Al_2O_3, hexanes) yielded 12.3 g (72.7%) of a light brown, glassy material. Purity (GPC), 99+%; TLC (10:1 hexanes:ethyl acetate): $R_f = 0.5$. ^{1}H NMR ($CDCl_3$, δ, ppm, TMS): 0.88 (t, 81H, CH_3(CH$_2$)$_{11}$, $J = 6.0$ Hz), 1.26−1.41 (overlapped peaks, 486H, CH$_3$(CH_2)$_8$), 1.71 (m, 54H, CH_2CH$_2$OAr), 3.66−3.91 (overlapped peaks, 57H, CH$_2$CH_2OAr, CO_2CH_3), 4.77 (bs, 4H, ArCH_2OAr, 4-(3′,5′) position), 4.81 (bs, 2H, ArCH_2OAr, 4-(4′) position), 4.91 (bs, 12H, ArCH$_2$OAr, 3,5-(3′,4′,5′) positions), 5.05 (bs, 4H, ArCH_2OAr, 3,5 positions), 5.12 (bs, 2H, ArCH_2OAr, 4 position), 6.51 (s, 6H, *ortho* to CH_2, 4-(3′,4′,5′) position), 6.57 (s, 12H, *ortho* to CH_2, 3,5-(3′,4′,5′) positions), 6.80 (s, 4H, *ortho* to CH_2, 3,5 positions), 6.85 (s, 2H, *ortho* to CH_2, 4 position), 7.38 (s, 2H, *ortho* to CO_2CH_3). ^{13}C NMR ($CDCl_3$, δ, ppm, TMS): 14.1 (*C*H$_3$), 22.7 (CH$_3$*C*H$_2$), 26.2 (*C*H$_2$CH$_2$CH$_2$OAr), 29.4 (CH$_3$(CH$_2$)$_2$*C*H$_2$), 29.8 (CH$_3$(CH$_2$)$_3$(*C*H$_2$)$_5$), 30.5 (*C*H$_2$CH$_2$OAr), 31.9 (CH$_3$CH$_2$*C*H$_2$), 52.2 (CO_2*C*H$_3$), 68.8, 68.9 (CH$_2$*C*H$_2$OAr, 3,4,5-[3′,4′,5′-(3″,5″)] positions), 71.4, 71.6 (Ar*C*H$_2$OAr, 3,5 positions and 3,4,5-(3′,5′) positions), 73.3 (CH$_2$*C*H$_2$OAr, 3,4,5-[3′,4′,5′-(4″)] positions), 75.1 (Ar*C*H$_2$OAr, 4 position and 3,4,5-(4′) positions), 105.5 (*ortho* to CH_2, 3,4,5-(3′,5′) positions), 105.9 (*ortho* to CH_2, 3,4,5-(4′) positions), 107.2 (*ortho* to CH_2, 3,5 positions), 108.0 (*ortho* to CH_2, 4 position), 109.6 (*ortho* to CO_2CH_3), 125.4 (*ipso* to CO_2CH_3), 131.8 (*para* to CH_2, 3,4,5-(3′,5′) positions), 132.3 (*para* to CH_2, 3,5 positions), 132.7 (*para* to CH_2, 3,4,5-(4′) positions), 133.1 (*para* to CH_2, 4 position), 137.7 (*ipso* to CH_2, 3,4,5-(3′,4′,5′) positions), 138.3 (*ipso* to CH_2, 3,4,5 positions), 142.2 (*para* to CO_2CH_3), 152.4 (*meta* to CO_2CH_3, *meta* to CH_2, 4 position), 152.8 (*meta* to CH_2, 3,5 positions), 153.0 (*meta* to CH_2, 3,4,5-(4′) positions), 153.2 (*meta* to CH_2, 3,4,5-(3′,5′) positions), 166.3 (*C*O$_2$-CH$_3$). Anal Calcd for $C_{416}H_{728}O_{41}$: C, 78.24; H, 11.49. Found: C, 78.31; H, 11.29.

3,4,5-Tris{3′,4′,5′-tris[3″,4″,5″-tris(*n*-dodecan-1-yloxybenzyloxy)-benzyloxy]benzyloxy}benzyl Alcohol (12G3-AG-CH_2OH). From **12G3-AG-CH_3** (7.0 g, 1.1 mmol) and $LiAlH_4$ (0.083 g, 2.2 mmol) was obtained 5.4 g (77%) of a glassy, white solid after purification by column chromatography (b. Al_2O_3; hexanes). Purity (GPC), 99+%. ^{1}H NMR ($CDCl_3$, δ, ppm, TMS): 0.88 (t, 81H, CH_3(CH$_2$)$_{11}$, J = 6.0 Hz), 1.26−1.44 (overlapped peaks, 486H, CH$_3$(CH_2)$_8$), 1.69 (m, 54H, CH_2CH$_2$OAr), 3.66−3.92 (overlapped peaks, 54H, CH$_2$CH_2OAr), 4.44 (d, 2H, CH_2OH, J = 6.5 Hz), 4.83 (bs, 4H, ArCH_2OAr, 4-(3′,5′) position), 4.85 (bs, 2H, ArCH_2OAr, 4-(4′) position), 4.93 (bs, 12H, ArCH$_2$OAr, 3,5-(3′,4′,5′) position), 4.98 (bs, 4H, ArCH_2OAr, 3,5 positions), 5.05 (bs, 2H, ArCH_2OAr, 4 position), 6.47 (s, 2H, *ortho* to CH$_2$OH), 6.52 (s, 6H, *ortho* to CH$_2$, 4-(3′,4′,5′) position), 6.56 (s, 8H, *ortho* to CH$_2$, 3,5-(3′,5′) positions), 6.60 (s, 4H, *ortho* to CH, 3,5-(4′) position), 6.73 (s, 4H, *ortho* to CH$_2$, 3,5 positions), 6.86 (s, 2H, *ortho* to CH$_2$, 4 position). ^{13}C NMR ($CDCl_3$, δ, ppm, TMS): 14.1 (*C*H$_3$), 22.7 (CH$_3$*C*H$_2$), 26.2 (*C*H$_2$CH$_2$CH$_2$OAr), 29.4 (CH$_3$(CH$_2$)$_2$*C*H$_2$), 29.8 (CH$_3$(CH$_2$)$_3$(*C*H$_2$)$_5$), 30.4 (*C*H$_2$CH$_2$OAr), 31.9 (CH$_3$CH$_2$*C*H$_2$), 64.7 (*C*H$_2$OH), 68.0, 68.9 (CH$_2$*C*H$_2$OAr, 3,4,5-[3′,4′,5′-(3″,5″)] positions), 71.4 (Ar*C*H$_2$OAr, 3,5 position and 3,4,5-(3′,5′) positions), 73.3 (CH$_2$*C*H$_2$OAr, 3,4,5-[3′,4′,5′-(4″)] positions), 75.2 (Ar*C*H$_2$OAr, 4 position and 3,4,5-(4′) positions), 105.4 (*ortho* to CH$_2$, 3,4,5-(3′,5′) positions), 106.0 (*ortho* to CH$_2$, 3,4,5-(4′) position), 106.6 (*ortho* to CH$_2$OH, *ortho* to CH$_2$, 3,5 positions), 108.3 (*ortho* to CH$_2$, 4 position), 132.0 (*para* to CH$_2$, 3,4,5-(3′,5′) positions), 132.8 (*para* to CH$_2$, 3,4,5-(4′) positions), 133.1 (*para* to CH$_2$, 3,5 positions), 133.6 (*para* to CH$_2$, 4 position), 136.9 (*ipso* to CH$_2$OH), 137.6 (*ipso* to CH$_2$, 3,4,5-(3′,4′,5′) positions), 137.9 (*ipso* to CH$_2$, 3,5 position), 138.2 (*ipso* to CH$_2$, 4 position), 152.6 (*meta* to CH$_2$OH, *meta* to CH$_2$, 4 position), 152.7 (*meta* to CH$_2$, 3,5 positions), 153.0 (*meta* to CH$_2$, 3,4,5-(4′) positions), 153.2 (*meta* to CH$_2$, 3,4,5-(3′,5′) positions).

3,4,5-Tris{3′,4′,5′-tris[3″,4″,5″-tris(*n*-dodecan-1-yloxybenzyloxy)-benzyloxy]benzyloxy}benzyl Chloride (12G3-AG-CH_2Cl). From **12G3-AG-CH_2OH** (0.90 g, 0.14 mmol), 2,6-di-*tert*-butylpyridine (78 mg, 0.40 mmol), and $SOCl_2$ (20 mg, 0.17 mmol) was obtained 0.90 g (100%) of a light yellow, glassy solid which was used without further purification. Complete conversion to the benzyl chloride (s, 2H, 4.45 ppm) and the absence of side reactions was verified by ^{1}H NMR analysis of the reaction mixture.

Methyl 3,4,5-Tris(3′,4′,5′-tris{3″,4″,5″-tris[3‴,4‴,5‴-tris(*n*-dodecan-1-yloxybenzyloxy)benzyloxy]benzyloxy}benzyloxy)benzoate (12G4-AG-CH_3). **12G4-AG-CH_3** was synthesized by the same general procedure described for the synthesis of **12G3-AG-CH_3** except that the reaction temperature was 80 °C. From K_2CO_3 (1.4 g, 10 mmol), methyl 3,4,5-trihydroxybenzoate (30.8 mg, 0.167 mmol), and **12G3-AG-CH_2Cl** (3.20 g, 0.502 mmol) in 32 mL of NMP (80 °C, 20 h) was obtained 1.60 g (50.0%) of a light brown, glassy solid after purification by column chromatography (b. Al_2O_3; hexanes). Purity (GPC), 99+%; TLC (hexanes), R_f = 0.9. ^{1}H NMR ($CDCl_3$, δ, ppm, TMS): 0.88 (broad peak, 243H, CH_3(CH$_2$)$_{11}$), 1.26 (broad peak, 1458H, CH$_3$(CH_2)$_8$), 1.71 (broad peak, 162H, CH_2CH$_2$OAr), 3.64−3.79 (broad peaks, 165H, CH$_2$CH_2OAr, CO$_2$CH_3), 4.76 (broad peak, 78H, ArCH_2OAr), 6.50 (broad peak, 54H, *ortho* to CH$_2$, 3,4,5-[3′,4′,5′-(3″,4″,5″)] positions), 6.81 (broad peak, 24H, *ortho* to CH$_2$, 3,4,5-(3′,4′,5′) and 3,4,5 positions). ^{13}C NMR ($CDCl_3$, δ, ppm, TMS): 14.1 (*C*H$_3$), 22.7 (CH$_3$*C*H$_2$), 26.2 (*C*H$_2$CH$_2$CH$_2$OAr), 29.4 (CH$_3$(CH$_2$)$_2$*C*H$_2$), 29.8 (CH$_3$(CH$_2$)$_3$(*C*H$_2$)$_5$ and *C*H$_2$CH$_2$OAr, 3,5 positions), 30.5 (*C*H$_2$CH$_2$OAr, 4 position), 31.9 (CH$_3$-CH$_2$*C*H$_2$), 52.2 (CO$_2$*C*H$_3$), 68.8 (CH$_2$*C*H$_2$OAr, 3,5 positions), 71.5 (Ar*C*H$_2$OAr, 3,5 positions), 73.2 (CH$_2$*C*H$_2$OAr, 4 positions), 74.9 (Ar*C*H$_2$OAr, 4 positions), 105.5 (*ortho* to CH$_2$, 3,4,5-[3′,4′,5′-(3″,4″,5″)] positions), 107.2 (*ortho* to CH$_2$, 3,4,5-(3′,4′,5′) and 3,4,5 positions), 130.3 (*ipso* to CO$_2$CH$_3$), 131.7 (*para* to CH$_2$, 3,4,5-[3′,4′,5′-(3″,4″,5″)] positions), 132.7 (*para* to CH$_2$, 3,4,5-(3′,4′,5′) position), 133.8 (*para* to CH$_2$, 3,4,5 positions), 137.7 (*ipso* to CH$_2$, 3,4,5-[3′,4′,5′-(3″,4″,5″)] positions), 138.2 (*ipso* to CH$_2$, 3,4,5-(3′,4′,5′) and 3,4,5 positions), 151.7 (*meta* to CO$_2$CH$_3$), 153.1 (*meta* to CH$_2$). Anal Calcd for $C_{1253}H_{728}O_{122}$: C, 78.36; H, 11.47. Found: C, 78.31; H, 11.29.

General Procedure for the Basic Hydrolysis of 12Gn-AG-CH_3 (n > 1). 3,4,5-Tris[3′,4′,5′-tris(*n*-dodecan-1-yloxy)benzyloxy)]benzoic Acid (12G2-AG). 12G2-AG-CH_3 (1.00 g, 0.473 mmol) was suspended in a mixture of 95% EtOH (10 mL) and 10 N KOH (1 mL), heated, and maintained at a gentle reflux for 3 h. After cooling to room temperature, EtOH was decanted, and the solid residue was dissolved in THF. The solution was neutralized with of 50% aqueous acetic acid. THF was added periodically to maintain a homogeneous solution. After acidification, the product was precipitated in acetone and collected by vacuum filtration. A white powder (0.88g, 88%) was obtained. Purity (GPC), 99+%; TLC (20:1 $CHCl_3$:MeOH), R_f = 0.33. ^{1}H NMR ($CDCl_3$, δ, ppm, TMS): 0.88 (t, 27H, CH_3(CH$_2$)$_{11}$, J = 6.4 Hz), 1.26−1.42 (overlapped peaks, 162H, CH$_3$(CH_2)$_8$), 1.71 (m, 18H, CH_2CH$_2$OAr), 3.75 (t, 4H, CH_2OAr, 4-(3′,5′) position, J = 6.4 Hz), 3.89 (t, 8H, 3,5-(3′,5′) positions, J = 6.4 Hz), 3.93 (t, 6H, CH$_2$OAr, 3,4,5-(4′) positions, J = 6.5 Hz), 5.04 (s, 6H, ArCH_2OAr), 6.60 (s, 2H, *ortho* to CH$_2$, 4 position), 6.64 (s, 4H, *ortho* to CH$_2$, 3,5 positions), 7.45 (s, 2H, *ortho* to CO$_2$H). ^{13}C NMR ($CDCl_3$, δ, ppm, TMS): 14.1 (*C*H$_3$), 22.7 (CH$_3$*C*H$_2$), 26.2 (*C*H$_2$CH$_2$CH$_2$OAr), 29.4 (CH$_3$(CH$_2$)$_2$*C*H$_2$), 29.7 (CH$_3$(CH$_2$)$_3$(*C*H$_2$)$_5$), 30.4 (*C*H$_2$CH$_2$OAr), 31.9 (CH$_3$CH$_2$*C*H$_2$), 69.1 (CH$_2$*C*H$_2$OAr, 3,4,5-(3′,5′) positions), 71.7 (Ar*C*H$_2$OAr, 3,5 positions), 73.4 (CH$_2$*C*H$_2$OAr, 3,4,5-(4′) positions), 75.2 (Ar*C*H$_2$OAr, 4 position), 105.8 (*ortho* to CH$_2$, 3,5 positions), 106.2 (*ortho* to CH$_2$, 4 position), 110.1 (*ortho* to CO$_2$H), 124.2 (*ipso* to CO$_2$H), 131.5 (*para* to CH$_2$, 3,5 positions), 132.3 (*para* to CH$_2$, 4 position), 137.9 (*ipso* to CH$_2$, 3,4,5 positions), 143.4 (*para* to CO$_2$H), 152.6 (*meta* to CO$_2$H), 153.0 (*meta* to CH$_2$, 4 position), 153.3 (*meta* to CH$_2$, 3,5 positions), 171.5 (*C*O$_2$H). Anal Calcd for $C_{136}H_{240}O_{14}$: C, 77.81; H, 11.52. Found: C, 78.03; H, 11.31.

3,4,5-Tris{3′,4′,5′-tris[3″,4″,5″-tris(*n*-dodecan-1-yloxybenzyloxy)-benzyloxy]benzyloxy}benzoic Acid (12G3-AG). From **12G3-AG-CH_3** (1.00 g, 0.157 mmol) was obtained 0.40 g (40%) of a white powder. Purity (GPC), 99+%; TLC (20:1 $CHCl_3$:MeOH), R_f = 0.68. ^{1}H NMR ($CDCl_3$, δ, ppm, TMS): 0.88 (t, 81H, CH_3(CH$_2$)$_{11}$, J = 6.0 Hz), 1.25 (overlapped peaks, 486H, CH$_3$(CH_2)$_8$), 1.68 (m, 54H, CH_2-CH$_2$OAr), 3.69−3.89 (overlapped peaks, 54H, CH$_2$CH_2OAr), 4.81 (bs, 4H, ArCH_2OAr, 4-(3′,5′) position), 4.83 (bs, 2H, ArCH_2OAr, 4-(4′) position), 4.91 (bs, 12H, ArCH$_2$OAr, 3,5-(3′,4′,5′) positions), 5.05 (bs, 4H, ArCH_2OAr, 3,5 positions), 5.12 (bs, 2H, ArCH_2OAr, 4 position), 6.52 (s, 4H, *ortho* to CH$_2$, 4-(3′,5′) position), 6.54 (s, 2H, *ortho* to CH$_2$, 4-(4′) position), 6.57 (s, 12H, *ortho* to CH$_2$, 3,5-(3′,4′,5′) positions), 6.75 (s, 4H, *ortho* to CH$_2$, 3,5 positions), 6.87 (s, 2H, *ortho* to CH$_2$, 4 position). ^{13}C NMR ($CDCl_3$, δ, ppm, TMS): 14.1 (*C*H$_3$), 22.7 (CH$_3$*C*H$_2$), 26.2 (*C*H$_2$CH$_2$CH$_2$OAr), 29.4 (CH$_3$(CH$_2$)$_2$*C*H$_2$), 29.8 (CH$_3$-(CH$_2$)$_3$(*C*H$_2$)$_5$), 30.5 (*C*H$_2$CH$_2$OAr), 32.0 (CH$_3$CH$_2$*C*H$_2$), 68.8, 68.9 (CH$_2$*C*H$_2$OAr, 3,4,5-[3′,4′,5′-(3″,5″)] positions), 71.6 (Ar*C*H$_2$OAr, 3,5 position and 3,4,5-(3′,5′) positions), 73.2 (CH$_2$*C*H$_2$OAr, 3,4,5-[3′,4′,5′-(4″)] positions), 75.1 (Ar*C*H$_2$OAr, 4 and 3,4,5-(4′) positions), 105.6 (*ortho* to CH$_2$, 3,4,5-(3′,5′) positions), 105.8 (*ortho* to CH$_2$, 3,4,5-(4′) positions), 107.2 (*ortho* to CH$_2$, 3,5 positions), 107.8 (*ortho* to CH$_2$, 4 position), 110.0 (*ortho* to CO$_2$H), 124.6 (*ipso* to CO$_2$H), 131.8 (*para* to CH$_2$, 3,4,5-(3′,5′) positions), 132.2 (*para* to CH$_2$, 3,5 positions), 132.7 (*para* to CH$_2$, 3,4,5-(4′) positions), 133.1 (*para* to CH$_2$, 4 position), 137.6, 137.7 (*ipso* to CH$_2$, 3,4,5-(3′,4′,5′) positions), 138.3 (*ipso* to CH$_2$, 3,4,5 positions), 143.0 (*para* to CO$_2$H), 152.5 (*meta* to CH$_2$, 4 position), 153.0 (*meta* to CH$_2$, 3,5 position), 153.2 (*meta* to CH$_2$, 3,4,5-(3′,4′,5′) positions), 169.8 (*C*O$_2$H). Anal Calcd for $C_{415}H_{726}O_{41}$: C, 78.22; H, 11.48. Found: C, 78.01; H, 11.30.

3,4,5-Tris(3′,4′,5′-tris{3″,4″,5″-tris[3‴,4‴,5‴-tris(*n*-dodecan-1-yloxybenzyloxy)benzyloxy]benzyloxy}benzyloxy)benzoic Acid (12G4-AG). Hydrolysis of **12G4-AG-CH_3** (1.4 g, 0.073 mmol) yielded 1.2 g (86%) of **12G4-AG1** after precipitation in acetone and subsequent purification by column chromatography (b. Al_2O_3; hexanes). Purity (GPC), 99+%; TLC (hexanes), R_f = 0.9. ^{1}H NMR ($CDCl_3$, δ, ppm, TMS): 0.88 (broad peak, 243H, CH_3(CH$_2$)$_{11}$), 1.26 (broad peak, 1458H, CH$_3$(CH_2)$_8$), 1.61 (broad peak, 162H, CH_2CH$_2$OAr), 3.66−3.80 (broad peaks, 162H, CH$_2$CH_2OAr), 4.78 (broad peak, 78H, ArCH_2OAr), 6.50 (broad peak, 54H, *ortho* to CH$_2$, 3,4,5-[3′,4′,5′-(3″,4″,5″)] positions), 6.82 (broad peak, 24H, *ortho* to CH$_2$, 3,4,5-(3′,4′,5′) and 3,4,5 positions). ^{13}C NMR ($CDCl_3$, δ, ppm, TMS): 14.0 (*C*H$_3$), 22.7 (CH$_3$*C*H$_2$), 26.3 (*C*H$_2$CH$_2$CH$_2$OAr), 29.4 (CH$_3$(CH$_2$)$_2$*C*H$_2$), 29.9 (CH$_3$(CH$_2$)$_3$(*C*H$_2$)$_5$), 30.6 (*C*H$_2$CH$_2$OAr), 32.0 (CH$_3$CH$_2$*C*H$_2$), 69.0 (CH$_2$*C*H$_2$OAr, 3,5 positions), 71.6 (Ar*C*H$_2$OAr, 3,5 positions), 73.2 (CH$_2$*C*H$_2$OAr, 4 positions), 74.9 (Ar*C*H$_2$OAr, 4 positions), 105.8 (*ortho* to CH$_2$, 3,4,5-[3′,4′,5′-(3″,4″,5″)] positions), 107.3 (*ortho* to CH$_2$, 3,4,5-(3′,4′,5′) and 3,4,5 positions), 131.8 (*para* to CH$_2$, 3,4,5-[3′,4′,5′-(3″,4″,5″)] positions), 132.8 (*para* to CH$_2$, 3,4,5-(3′,4′,5′) positions), 133.8 (*para* to

CH_2, 3,4,5 positions), 137.8 (*ipso* to CH_2, 3,4,5-[3′,4′,5′-(3″,4″,5″)] positions), 138.3 (*ipso* to CH_2, 3,4,5-(3′,4′,5′) and 3,4,5 positions), 151.7 (*meta* to CO_2H), 153.2 (*meta* to CH_2), 169.5 (CO_2H). Anal Calcd for $C_{1252}H_{2184}O_{122}$: C, 78.36; H, 11.47. Found: C, 78.50; H, 11.40.

Acknowledgment. The authors wish to acknowledge financial support from the National Science Foundation, U.S.A. (DMR-92-06781), the Engineering and Physical Science Research Council, UK, and the Synchrotron Radiation Source at Daresbury, UK (for the beamtime and technical assistance). A NATO traveling grant is also acknowledged. We are grateful to Professor S. Z. D. Cheng of University of Akron for supplying the mass density data and Dr. Charles McEwen of Central Research Department, DuPont, Wilmington, for providing the preliminary data on MALDI-TOF MS.

Supporting Information Available: Schematic drawing of five cubic phases, MALDI-TOF spectra, NMR data and spectra, DSC traces, powder and monodomain X-ray diffractograms, electron density profiles, and histograms for **12G2-AG** and their discussion, and principles of phase formation by different curvature (15 pages). See any current masthead page for ordering and Internet access instructions.

JA963295I